An Experimental Investigation of Fracture at a Bimaterial Interface

Thesis by

John Murray Bowen

In Partial Fulfillment of the Requirements

for the Degree of

Aeronautical Engineer

California Institute of Technology

Pasadena, California

1992

(submitted May 6, 1992)

To my wife, my mum and dad, and my siblings,

for all of their love, support, and encouragement.

Acknowledgements

This work was made possible through the support, guidance and encouragement of many people. Chief among these was my advisor, Professor Wolfgang G. Knauss, who provided scientific direction when needed, valuable suggestions when appropriate, and continuous support throughout my graduate studies.

I would like to acknowledge principal support from the Air Force under contract F04611-88-K-0024, with technical guidance provided by Dr. Chi-Tsieh Liu, and additional support from ONR Grant N00014-91-J-1427, under the direction of Dr. Peter Schmidt. The direct and indirect assistance provided by these gentlemen and the organizations they represent are greatly appreciated.

I wish to acknowledge the significant contributions made towards this research effort by Mr. Eli Mazor. Both the specimen preparation technique and the experimental procedure outlined here are largely the outgrowth of Mr. Mazor's preliminary work with Solithane during his tenure as Visiting Associate at Caltech from 1989-90.

Special thanks are in order for my colleague and friend, Philippe Geubelle, who provided valuable insight through informative discussions on countless occasions. Mr. Geubelle's guidance has really been phenomenal.

I would also like to acknowledge the skills and services of George Lundgren, Larry Frazier, and Phil Wood of the Aeronautics Machine Shop. In particular, I thank Mr. Frazier for his exceptional assistance in machining the specimens used in this study.

Finally, I would like to thank all the friends I've made here for providing camaraderie and welcomed diversions. Also, special thanks to the guys at SURFLINE for encouraging many, if not most, of the aforementioned diversions.

I especially want to thank my wonderful wife, Jennifer, for her patience and support throughout what began, innocently enough, as a "1 year Master's."

Abstract

The growth of a crack located at the interface between two linearly (visco)elastic solids is investigated experimentally. It is found that the crack may advance by kinking into either of the adherends or by propagating along the interface itself, depending on the applied loading. For the separation problem, in which crack advance occurs along the bimaterial interface, it is demonstrated that the time-dependent unbonding of the two joined viscoelastic solids follows a rate-dependent fracture process that can be described to a large extent by the viscoelastic properties of the two adherends. Moreover, the strength of the interfacial bond can be characterized in terms of an equilibrium interface-intrinsic fracture energy, the magnitude of which represents the bond strength quantitatively. In particular, interface strength on the same order as those of the adherends is achieved. In contrast to the time-dependent approach developed for the separation problem, the propensity of the interface crack to kink out of the interface upon loading is evaluated in the context of (time-independent) linearly elastic fracture mechanics. It is demonstrated that crack propagation along the interface occurs for a finite range of load mixity, a phenomenon predicted by linear analysis of the bimaterial joint but absent from the corresponding homogeneous development. Agreement between observed kinking behavior and analytical results is seen to improve by suitable manipulation of a presumably material characteristic length, the origin of which is rooted in the linearized analysis. The influence of material rate effects on the crack kinking behavior is also investigated.

Table of Contents

List of Figures

List of Tables

CHAPTER 1

Introduction

Many engineering applications require the joining of two dissimilar materials. Often, these joints are intended to work either primarily or accessorily as failure barriers; that is, they are intended to prevent the propagation of cracks beyond the joint should a failure occur. In solid propellant rocket motors, for example, the interface between the liner and the insulation should be invulnerable to cracks that may originate in the propellant (Fig. 1.1). In the event that such a crack does damage the integrity of the insulating layer, which protects the motor case from the extreme temperatures developed during motor operation, burn-through of the motor case and possible catastrophic failure may result. Thus, for design purposes, an understanding of interfacial and near-interfacial crack propagation behavior is essential.

This study is concerned with an experimental method for characterizing the fracture behavior of an interface crack within a bimaterial joint that is subjected to various "far-field" loading conditions. In particular, the focus here is on observing and delineating the propensity of the crack to kink out of the interface and propagate into either of the adjacent materials according to the near-tip conditions. The near-tip conditions, characterized by a complex-valued stress intensity factor, are taken as the prescribed loading parameters in this study and are dictated by the applied far-field load and the specimen geometry. Following the convention established to describe the fracture of homogeneous bodies, linearly elastic fracture mechanics,

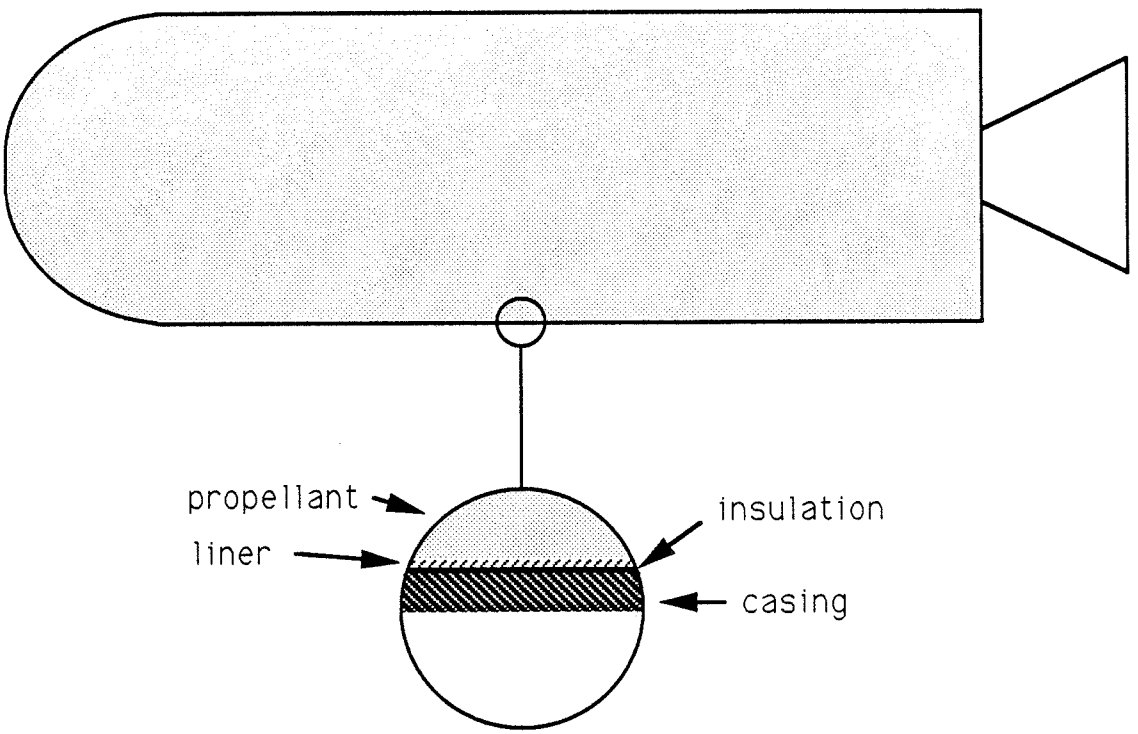

FIG. 1.1 A solid propellant rocket motor.

with all its underlying assumptions, is applied. For simplicity, quasi-static crack growth conditions are enforced.

The strength or toughness of the interface between the two solids has a profound influence on the ultimate fracture behavior of the bimaterial joint. Thus, prerequisite for a comprehensive investigation of interfacial crack kinking behavior is an evaluation of the strength of the bond that exists between the two materials. Because the model materials chosen for this study exhibit time-dependent material behavior, it is appropriate to examine the toughness of the interface in the context of viscoelasticity. It is expected that the experimental characterization of interfacial fracture toughness presented in this thesis may shed new light on the mechanics of bondline decohesion. To provide the background required for this toughness evalu-

ation, the theory of viscoelastic bondline decohesion is introduced in Ch. 2.[1]

The most fundamental geometry for analyzing the bimaterial fracture problem involves two dissimilar, isotropic elastic solids with a crack lying at the planar interface between them (Fig. 1.2). The materials are considered to be joined together directly, without the aid of a third, adhesive agent. The analytical solution to this boundary value problem was first developed by Williams (1959) in terms of an eigenfunction expansion. A review of the procedure followed by Williams is presented and discussed in Ch. 3. The primary concepts of linearly elastic fracture mechanics as they apply to the interfacial crack problem are also cited. These concepts include the form of the stress and displacement fields in the vicinity of the crack tip, the complex stress intensity factor, and a criterion for assessing the propensity of the crack to kink out of the interface.

The work presented in this thesis is primarily experimental in nature. For this investigation, the geometry of Fig. 1.2 is incorporated into a planar, thin-sheet specimen that permits the analytical simplifications inherent in plane stress problem formulations (Fig. 1.3). Of paramount importance in the physical test specimen is the integrity of the interface between the two solids. Ideally, this interface should be planar (*i.e.*, "flat") in order to parallel the typical analytical modelling of the problem, and of sufficient strength to prevent invariable decohesion along the bondline upon loading. The procedure followed to manufacture bimaterial fracture specimens that meet these criteria is presented in Ch. 4.

---

[1] Inasmuch as the model materials employed in this study do indeed exhibit time-dependent material response, it is prudent to question the applicability of (time-independent) elasticity theory to the kinking aspect of interfacial fracture. However, the prevailing point of view maintains that the influence of rate effects on the kinking behavior is expected to be minor in comparison to the effect of the shear/tension interaction at the tip of the crack. Moreover, as a consequence of the time-temperature trade-off inherent in viscoelastic material behavior, the validity of this assumption is readily checked by performing duplicate tests at different temperatures, thereby isolating the influence of rate effects on the resulting fracture behavior.

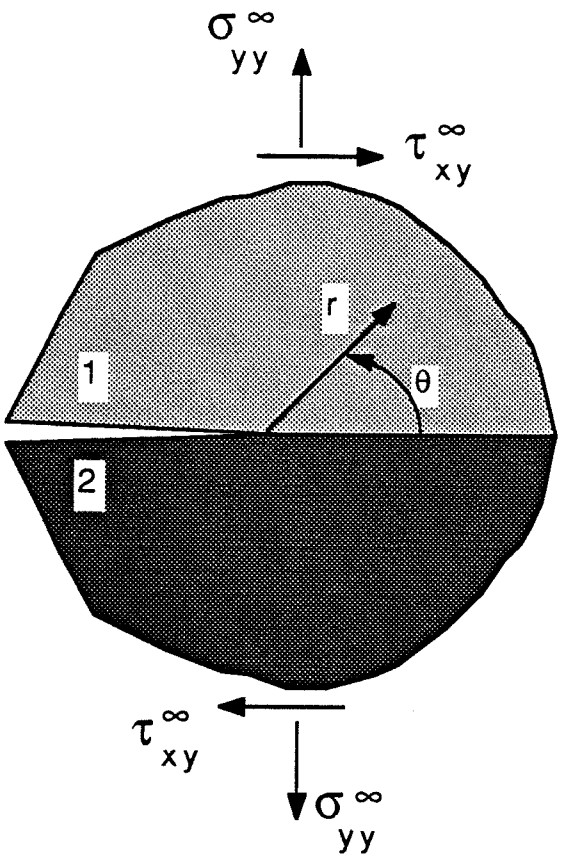

FIG. 1.2 Geometry of the bimaterial problem.

Chapter 5 is concerned with the experimental set-up and the procedure followed in obtaining fracture test results. In that chapter, the load frame utilized to remotely impose combined tension and shear loadings is presented. By utilizing finite element techniques, the near-tip conditions due to the prescribed far-field loading can be assessed within the framework of small deformation elasticity. The finite element mesh and the code exploited for this determination are cited in Ch. 5.

The experimental results are presented and discussed in Ch. 6. First of all, the rate-dependent fracture toughness of each of the joined solids is obtained and examined. These findings are analyzed in the context of viscoelastic monolithic fracture and viscoelastic bondline decohesion; then, the observed rate-dependence of fracture along the bimaterial interface is compared with the behavior predicted by the

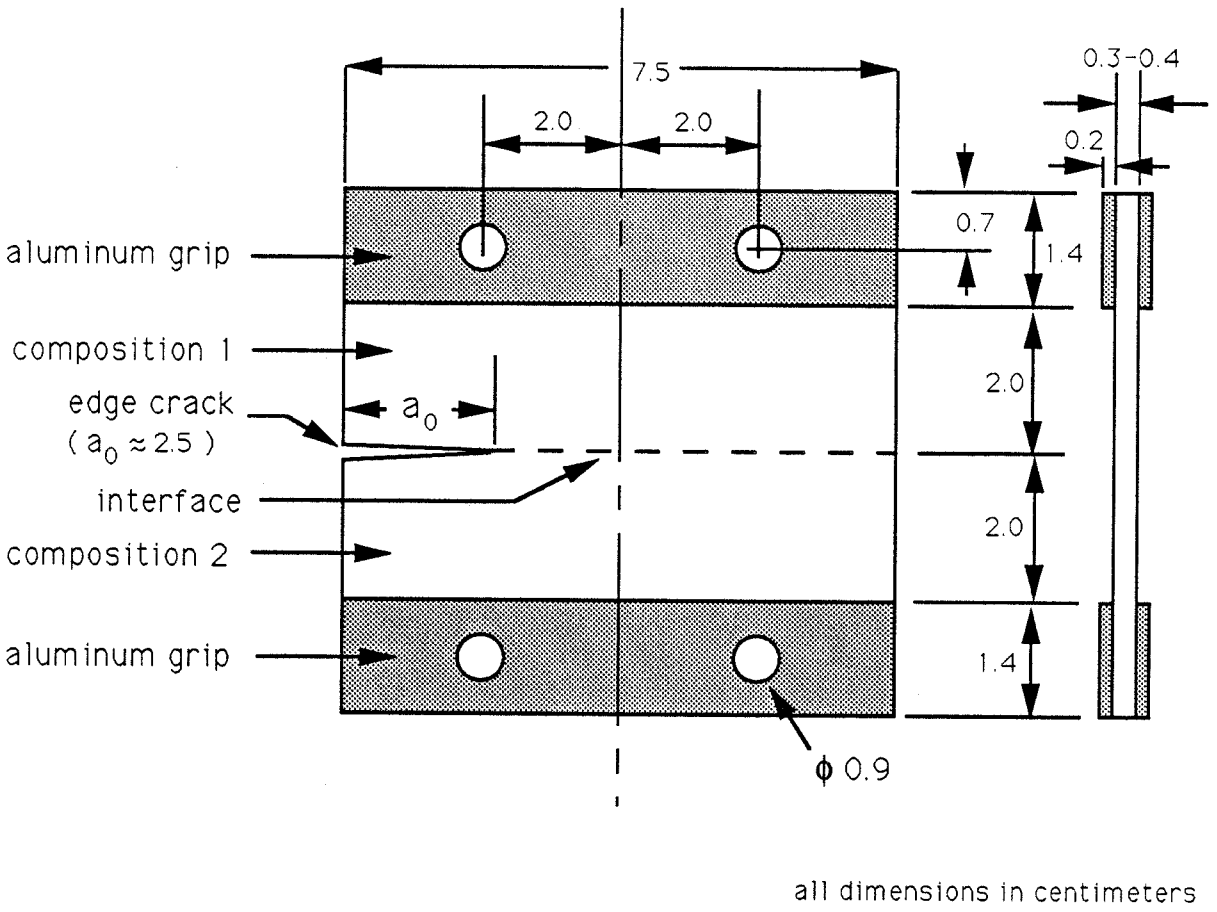

FIG. 1.3 Specimen geometry for experimental characterization.

theory. Secondly, the observed kinking behavior of the interface crack is presented. These latter results constitute a significant and comprehensive body of physical evidence regarding the propensity of a crack to kink out of an interface according to the character of the near-tip stress field. The influence of rate effects on the kinking behavior is investigated by performing fracture tests at elevated temperature, thereby accelerating the material response to the applied load. For completeness, the experimental results are compared with various analytical predictions.

In Ch. 7, conclusions are drawn from the research presented in this thesis. Also discussed in that last chapter are recommendations for future work on this complex problem.

CHAPTER 2

Viscoelastic Bondline Decohesion

2.1 Introduction

There are two fundamental objectives of fracture mechanics. The first goal is the determination of the resistance of a structure to fracture: For a body with a given flaw or crack size, fracture mechanics principles should provide an estimate of the maximum load which can be sustained by the body without fracture being induced. For a viscoelastic solid, it will also be necessary to establish the rate at which the flaw growth proceeds. This latter requirement stems from the fact that crack growth may occur so slowly that the integrity of the structure is not jeopardized throughout the course of its intended service life. The second aim of fracture mechanics is to predict the trajectory of crack advance: Given that failure by crack advance is imminent, fracture mechanics should be capable of reliably predicting the path of the propagating crack under known loading conditions. For composite structures, such predictions are complicated by the non-homogeneities and interfaces inherent in such materials; nevertheless, such analyses are essential to the design of critical parts that can not tolerate significant crack advance should a flaw arise in service.

These two objectives are, of course, very intimately related. Nevertheless, the two goals can be effectively separated, especially under laboratory conditions. The primary focus of this particular investigative effort is on delineating the behavior of an interface crack that is subjected to far-field loading that ensures stable (quasi-static) crack growth. Given that the crack will advance, the fundamental aim of this study is to characterize the emerging fracture path. However, because the strength of the interface exerts a profound influence on the ultimate fracture behavior of the bimaterial joint, it is essential to also characterize the toughness of the interface, *i.e.*, its resistance to fracture. Thus, consideration of both aspects of fracture mechanics is required in this study. The first objective outlined above is addressed in this chapter; the second is discussed in Ch. 3.

Inasmuch as the two solids which comprise the bimaterial specimen exhibit time-dependent material behavior, the interface toughness must be assessed in the context of viscoelasticity. A consequence of this formulation is that the rate of crack propagation is contingent upon the magnitude of the applied load. This situation will be elucidated in the following section.

It is appropriate at this time to emphasize that this initial analysis of interfacial crack propagation behavior is restricted to the most elementary conditions possible. Although one is ultimately interested in characterizing the fracture behavior resulting from arbitrary, time-varying boundary conditions, it is advantageous to first thoroughly investigate the fundamental problem of quasi-static crack growth under constant loading conditions. Consequently, neither the starting transients associated with the applied loading, nor the mechanics of crack growth initiation, shall be addressed here.

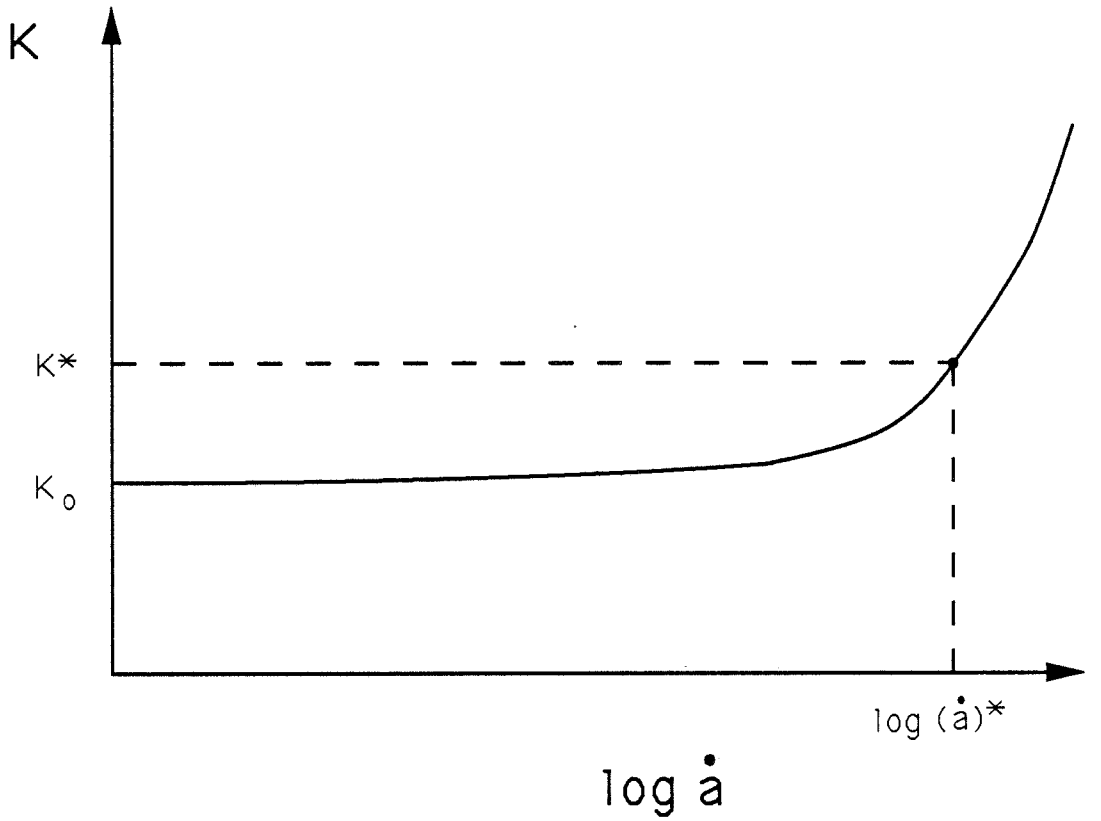

FIG. 2.1 Rate-dependent fracture toughness of a homogeneous viscoelastic material.

2.2 Rate-Dependent Fracture Toughness

A typical plot of stress intensity factor K (or alternatively, energy release rate $\mathcal{G}$) *vs.* crack speed $\dot{a}$ for a homogeneous, viscoelastic solid has the form shown in Fig. 2.1. The shape of this curve incorporates the rate effects of the material surrounding the moving crack tip during a fracture process.

Consider a point $((\dot{a})^*, K^*)$ on the "knee" of the curve. As the load level is increased beyond K^*, the material responds with faster and faster crack propagation rates. Eventually, kinetic effects become important and the assumptions inherent in a quasi-static problem formulation become invalid. On the other hand, as the load level is decreased from K^*, the resulting crack speed decreases. As the

asymptotic value represented by K_0 is approached from above, the rate of crack advance decreases to imperceptible levels, and the crack can be considered stationary. Note also that load levels less than those represented by K_0 are too low to allow crack advance. In terms of the energy associated with crack advance, for load levels below K_0, the energy available for crack advance is insufficient to overcome the energy required (this latter energy quantifies the toughness of the material) and the crack cannot grow. Thus, the horizontal asymptote of the curve illustrated in Fig. 2.1 represents the intrinsic fracture strength of the material; it is conceived of as a material constant.

For values of K greater than K_0, the curve in Fig. 2.1 embodies the rate effects exhibited by the material. Specifically, the shape of the "knee" characterizes the influence of the material rate sensitivity on the fracture behavior of the solid. For this reason, the type of plot depicted in Fig. 2.1 shall be referred to as a "rate-dependent fracture toughness diagram." In the following development, the rate dependence shall be isolated from the intrinsic, rate-independent fracture toughness of the material. The wisdom of this approach will become apparent when the problem of interfacial separation is ultimately addressed in a later section.

In general, a rate-dependent fracture toughness plot can be calculated for a given material from the general equation for crack growth. For the limiting case in which the loads acting on a (nearly) incompressible fracturing body do not change suddenly, Knauss (1974) has demonstrated that this equation is given by

$$2D^{\infty}\Theta\left(\frac{\alpha}{\dot{a}}\right)K^2 = \Gamma \text{ (plane stress)}, \tag{2.2.1}$$

where $D^{\infty} = D(\infty)$ is the long-term or equilibrium uniaxial creep compliance of the homogeneous solid, $\Theta(s)$ is a viscoelasticity function defined below, α is a characteristic, microstructural parameter (representative of the length over which material

disintegration takes place during crack advance)[1], a and $\dot{a}$ are the crack length and crack tip velocity, respectively, K is the crack tip stress intensity factor, and Γ represents the intrinsic, constant surface energy required for unit crack extension into the material in the limit of (near) zero crack speed (*i.e.*, in the absence of viscoelastic effects).[2]

Equation 2.2.1 strictly applies only in the case of constant crack speed. However, this equation also applies with good approximation to varying crack speeds provided that the condition

$$\frac{1}{K}\frac{\partial K}{\partial t} \ll \frac{\dot{a}(t)}{2\alpha(t)} \tag{2.2.3}$$

is always met. Under these circumstances, $K = K(t)$ is the time-varying stress intensity factor [Knauss and Dietmann (1970), Knauss (1976)].

The function $\Theta(s)$ is defined in terms of the uniaxial creep compliance $D(t) = D_0 + \Delta D(t)$ ($D_0 = D(0) = \text{const.}$) by

$$\Theta(s) = E^{\infty}\int_0^1 \left\{ D_0 F(\rho) - \int_\rho^1 \Delta D[s\cdot(r-\rho)]\frac{dF(r)}{dr}dr \right\} d\rho, \tag{2.2.4}$$

where $E^{\infty} = 1/D^{\infty}$ is the long-term or equilibrium uniaxial modulus of elasticity, and $F(r)$ is a non-dimensional function related to the crack tip stress field and deformation.[3] Conveniently, the function $\Theta(s)$ is well approximated by the simple

---

[1] In a polyurethane similar to that studied here [Knauss (1974)], α was found to make the experimental data fit Eq. 2.2.1 excellently if it was identified with the Dugdale/Barenblatt parameter

$$\alpha \equiv \frac{\pi K^2}{8\sigma_0^2} \tag{2.2.2}$$

in which σ_0 denotes the ultimate cohesive stress of the solid.

[2] For plane strain conditions, simply replace Γ by $\Gamma/(1-\nu^2)$ in Eq. 2.2.1; also carry out this substitution for Γ in all subsequent equations containing this term.

[3] In light of the forthcoming approximation to $\Theta(s)$ and the subsequent abandonment of $F(r)$, the form of this latter expression is omitted; the reader is referred to the work by Knauss (1974) for a thorough discussion of this equation.

expression

$$\Theta(s) \doteq \frac{1}{2} E^{\infty} D(s), \tag{2.2.5}$$

as shown by Knauss (1974) and implicit in the work of several investigators [Knauss (1976), Knauss and Dietmann (1970), Knauss and Mueller (1971), and Schapery (1975)]. Accordingly, Eq. 2.2.1 may be rewritten (approximately) as

$$D\left(\frac{\alpha}{\dot{a}}\right) K^2 = \Gamma. \tag{2.2.6}$$

It is convenient to introduce here the function $\Psi(\frac{\alpha}{\dot{a}})$, defined by

$$\Psi(\frac{\alpha}{\dot{a}}) \equiv \frac{1}{2\Theta(\frac{\alpha}{\dot{a}})}. \tag{2.2.7}$$

This function possesses, by virtue of Eq. 2.2.5, the limit $\Psi(\infty) = \frac{1}{2\Theta(\infty)} = 1$; $\Psi(s)$ is the time or velocity dependent component of the fracture energy determined from experiments, as shown later (in Ch. 6). With $\Psi(s)$ thus defined, Eq. 2.2.1 may now be written as

$$D^{\infty} K^2 = \frac{K^2}{E^{\infty}} = \Gamma \cdot \Psi(\frac{\alpha}{\dot{a}}). \tag{2.2.8}$$

One recognizes in the left hand side of Eq. 2.2.8 that combination of terms identified in linearly elastic fracture mechanics as the energy release rate for the solid in its globally relaxed state. Furthermore, the right hand side represents the fracture energy, or toughness, of the solid; in the present context, this energy depends on the speed of crack propagation. It should be noted that this rate-dependent fracture toughness is represented by a multiplicative operation of the time or rate (velocity) dependent function $\Psi(s)$ and the intrinsic, rate-independent fracture energy (fracture toughness) Γ. This combination of terms has been postulated before to represent a rate-dependent fracture energy [Knauss (1974), and Greensmith (1956, 1960)].

2.3 Rate-Dependent Interface Separation

For the case of two nearly incompressible viscoelastic solids joined together, Knauss (1971) has proposed that the rate of unbonding along the interface is governed (approximately) by

$$\left[D_1^{\infty}\Theta_1\left(\frac{\alpha}{\dot{a}}\right) + D_2^{\infty}\Theta_2\left(\frac{\alpha}{\dot{a}}\right)\right]K^2 = \Gamma_i, \tag{2.3.1}$$

where D_1^{∞} and D_2^{∞} are the long-term creep compliances of the two joined solids, $\Theta_1(s)$ and $\Theta_2(s)$ are the appropriate viscoelastic functions of Eq. 2.2.4, $K^2 = K_1^2 + K_2^2$ (where K_1 and K_2 represent approximately the local mode I and mode II stress intensity factors[4]), and Γ_i represents the intrinsic strength of the interface (intrinsic fracture energy). One notes that, because of Eq. 2.2.5, the factor multiplying K^2 represents, with very good approximation, the average of the two material compliances. In this formulation, the length scale α is that which is appropriate for the debonding problem. However, it is not clear at this time how that length scale is related to those associated with the two homogeneous materials by themselves. In fact, there is little hope at present that on the basis of linearly (visco)elastic fracture analysis such a general relation could be established analytically: Problems associated with the pathological behavior of the crack tip stress field seem to preclude such expectations [Geubelle and Knauss (1991)]. Nevertheless, in the interest of further pursuing this problem, it is assumed that the size scales for the two solids studied here are sufficiently close so as not to pose a problem of first order. In effect, it is assumed then that the interface failure is governed approximately by the same size parameter as for the two materials separately. This expectation is

[4] The stress intensity factors appropriate to the bimaterial fracture problem will be discussed in the following chapter. For clarity of presentation in this section, a discussion of the details of the "oscillatory character" of the stress field at the tip of an interface crack is circumvented here. Also, it should be noted that this development is limited to the case of (nearly) incompressible materials under plane stress conditions. Thus, Poisson's ratio should always approach 1/2.

based on the fact that the experimental data presented here are obtained from two polyurethanes, the molecular structures of which are not very different. It would be appropriate in a follow-on study to examine the consequences of employing a more distinctly different set of materials (after one has learned how to control the interface strength of such a material combination).

After slight algebraic manipulation, Eq. 2.3.1 can be cast in terms of functions and material parameters that describe the fracture of each of the two homogeneous solids that comprise the bimaterial body:

$$\frac{1}{2}\left(D_1^{\infty}+D_2^{\infty}\right)K^2=\Gamma_i\left[\frac{D_1^{\infty}+D_2^{\infty}}{2D_1^{\infty}\Theta_1\left(\frac{\alpha}{\dot{a}}\right)+2D_2^{\infty}\Theta_2\left(\frac{\alpha}{\dot{a}}\right)}\right]. \tag{2.3.2}$$

One notes in passing that this expression yields the elastic limit case in the event of vanishing crack speeds when the bracketed factor on the right hand side, which multiplies Γ_i, tends to unity. By analogy (*cf*. Eq. 2.2.8), this bracketed expression is denoted by Ψ_i, the velocity dependent function appropriate to the interface itself:

$$\Psi_i\left(\frac{\alpha}{\dot{a}}\right)=\frac{D_1^{\infty}+D_2^{\infty}}{2D_1^{\infty}\Theta_1\left(\frac{\alpha}{\dot{a}}\right)+2D_2^{\infty}\Theta_2\left(\frac{\alpha}{\dot{a}}\right)}=\frac{D_1^{\infty}+D_2^{\infty}}{\left(\frac{D_1^{\infty}}{\Psi_1(s)}\right)+\left(\frac{D_2^{\infty}}{\Psi_2(s)}\right)}. \tag{2.3.3}$$

Hence Eq. 2.3.2 becomes

$$\frac{1}{2}\left(D_1^{\infty}+D_2^{\infty}\right)K^2=\Gamma_i\cdot\Psi_i\left(\frac{\alpha}{\dot{a}}\right). \tag{2.3.4}$$

Thus it is postulated that Eqs. 2.3.3 and 2.3.4 describe fracture along the interface between two viscoelastic solids. Again (*cf*. Eq. 2.2.8), the left hand side of Eq. 2.3.4 is identified in linearly elastic fracture mechanics as the energy release rate for the solid in its globally relaxed state; the right hand side represents the rate-dependent

fracture energy, or toughness, of the interface itself. As in the case of the fracture of a homogeneous viscoelastic body, the rate-dependent fracture toughness of the interface is described by a multiplicative operation of the inherent, rate-independent toughness Γ_i and the rate-dependent function $\Psi_i(s)$.

The rate-dependent function Ψ_i embodies the material rate effects of interfacial separation. It is interesting to note that the above development suggests that Ψ_i is not strictly a property of the interface itself, but rather a composite function of the material behavior exhibited by the two homogeneous solids on either side of the interface. (By virtue of Eq. 2.3.3, the function Ψ_i is completely specified in terms of the material parameters which describe the fracture of each of the two adherends separately; thus, the integrity of the interfacial bond itself is irrelevant to the value of Ψ_i.) In contrast, the intrinsic interface fracture energy Γ_i is a property of the bondline itself. This latter parameter characterizes the (minimum) strength of the interface and its magnitude depends solely on the quality and integrity of the molecular bond that is obtained between the two solids that comprise the joint. It is conjectured that this property of the interface is dependent upon the molecular structure of the interfacial region, analogous to the way in which the fracture energy of each homogeneous body depends on its molecular make-up [Lake and Thomas (1967)].

For completeness of presentation, consider a special case, namely when one of the solids (say, for example, solid "2") is rigid. In that event, Eq. 2.3.4 reverts to

$$\frac{K^2}{E_1^\infty} = 2\Gamma_i \frac{1}{2\Theta_1\left(\frac{\alpha}{\dot{a}}\right)} = 2\Gamma_i \cdot \Psi_1\left(\frac{\alpha}{\dot{a}}\right). \tag{2.3.5}$$

This latter equation indicates that the time-dependent failure of a polymer-rigid interface follows the same fracture law as that of a homogeneous viscoelastic solid

(*cf*. Eq. 2.2.8), except that in the (bimaterial) separation case, the intrinsic fracture energy is replaced by twice the interface fracture energy. One explanation for the factor of two is rooted in the observation that energy release is provided by only half of the solid that would make up the homogeneous problem. From a practical point of view, the factor is often irrelevant, particularly in cases where Γ_i is not known separately from a series of independent fracture tests.

An application of the above theoretical development is deferred to the portion of this thesis concerned with experimental results, *viz.*, Ch. 6. In that chapter, a pedagogical application of the equations developed above will help illustrate the methodology implicit in this development.

CHAPTER 3

Linearly Elastic Interfacial Fracture Mechanics

3.1 Introduction

The principal focus of this investigative effort is on characterizing the behavior of an interface crack that is subjected to far-field loading that ensures stable (quasi-static) crack growth. Given that the crack will advance, one aim is to characterize the emerging fracture path. Ultimately, it is expected that this research will provide an answer to the deceptively simple question: How do the applied loads affect the direction of crack propagation relative to the interface?

While the question is fundamental, it must be recognized that the mechanics of interfacial fracture are very complex. Indeed, the transition of linearly elastic fracture mechanics concepts from homogeneous solids to interfacial geometries in bimaterial solids is not as smooth as one might anticipate. In fact, the "solution" to the bimaterial problem formulation seems to raise more questions than it helps to answer. It is precisely for this reason that a comprehensive experimental program concerned with providing physical data on the crack growth behavior needs to be performed. However, before the experimental program can be properly designed and articulated, the fundamental analytical concepts of linearly elastic interfacial fracture mechanics (LEIFM) need to be explored and clarified. The aim of this chapter is to provide this conceptual background.

It is appropriate at this time to remind the reader that this analysis is restricted to the most elementary conditions possible. Thus the loading parameters are maintained constant and quasi-static crack growth conditions are enforced. Moreover, neither the starting transients associated with the applied loading, nor the mechanics of crack growth initiation, shall be addressed here.

3.2 The Williams Solution

This section begins with an outline of Williams' (1959) method for obtaining the linearly elastic fields near the tip of a crack located at the interface between two dissimilar media. The geometry analyzed is that of the planar, semi-infinite interface crack introduced in Fig. 1.2. For convenience, this figure is reproduced here as Fig. 3.1.

The approach developed by Williams involves the determination of a biharmonic stress function $\chi(r,\theta)$ that ensures continuity of displacements and stresses across the interface ($\theta = 0$) and provides that the normal and shear stresses, $\sigma_{\theta\theta}$ and $\tau_{r\theta}$, vanish along the crack faces ($\theta = \pm\pi$).

Recall that the biharmonic stress function $\chi(r,\theta)$ must satisfy

$$\nabla^4 \chi(r,\theta) = 0. \tag{3.2.1}$$

For the bimaterial problem, two stress functions are, in fact, required - one for each medium. Following the notation of Symington (1987) and allowing the eigenvalues λ_c to be complex-valued, typical solutions to Eq. 3.2.1 are chosen of the form

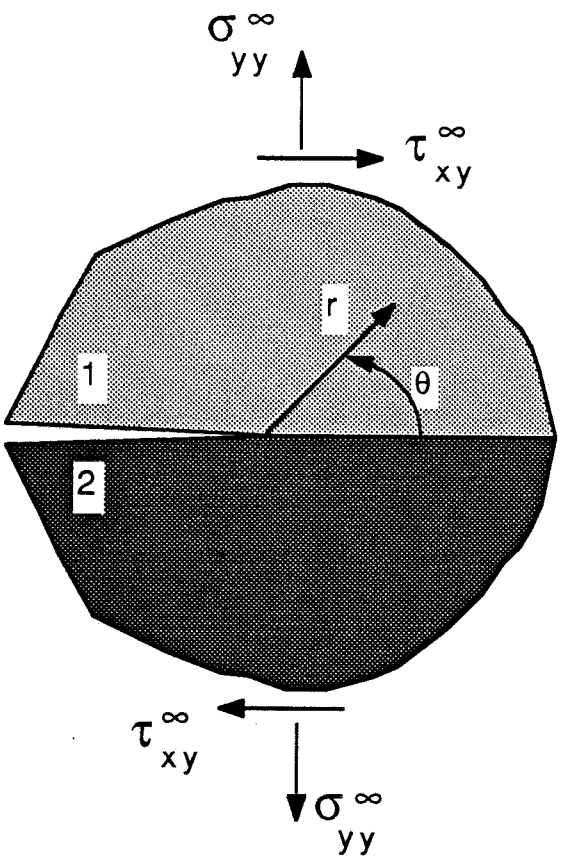

FIG. 3.1 Geometry of the bimaterial problem.

$$\chi_\alpha(r,\theta) = \Re e\{r^{\lambda_c+1} F_\alpha(\theta)\}, \tag{3.2.2a}$$

where

$$\begin{aligned} F_\alpha(\theta) = {} & a_\alpha \sin(\lambda_c+1)\theta + b_\alpha \cos(\lambda_c+1)\theta \\ & + c_\alpha \sin(\lambda_c-1)\theta + d_\alpha \cos(\lambda_c-1)\theta \end{aligned} \tag{3.2.2b}$$

and the subscript $\alpha = 1, 2$ identifies the material as indicated in Fig. 3.1.

The relations between the stresses and the stress function thus become

$$\sigma_{rr} = \frac{1}{r^2}\frac{\partial^2 \chi_\alpha}{\partial \theta^2} + \frac{1}{r}\frac{\partial \chi_\alpha}{\partial r} = r^{\lambda_c - 1}[F_\alpha''(\theta) + (\lambda_c+1)F_\alpha(\theta)] \tag{3.2.3a}$$

$$\sigma_{\theta\theta} = \frac{\partial^2 \chi_\alpha}{\partial r^2} = r^{\lambda_c - 1} \lambda_c (\lambda_c + 1) F_\alpha(\theta) \tag{3.2.3b}$$

and

$$\tau_{r\theta} = -\frac{1}{r}\frac{\partial^2 \chi_\alpha}{\partial r \partial \theta} + \frac{1}{r^2}\frac{\partial \chi_\alpha}{\partial \theta} = -\lambda_c r^{\lambda_c - 1} F'_\alpha(\theta), \tag{3.2.3c}$$

where the primes denote differentiation with respect to θ. The displacements are given in terms of the stress function by

$$u_r = -\frac{1}{2\mu_\alpha} r^{\lambda_c} \left((\lambda_c + 1) F_\alpha(\theta) - 4 \left(\frac{1}{1 + \nu_\alpha} \right) [c_\alpha \sin(\lambda_c - 1)\theta + d_\alpha \cos(\lambda_c - 1)\theta] \right) \tag{3.2.4a}$$

and

$$u_\theta = -\frac{1}{2\mu_\alpha} r^{\lambda_c} \left(F'_\alpha(\theta) + 4 \left(\frac{1}{1 + \nu_\alpha} \right) [c_\alpha \cos(\lambda_c - 1)\theta - d_\alpha \sin(\lambda_c - 1)\theta] \right), \tag{3.2.4b}$$

where μ is the shear modulus and ν is the Poisson ratio.

It is important to note that the relationship $(\lambda_c)_1 \equiv (\lambda_c)_2 \equiv \lambda_c$ used implicitly in Eqs. 3.2.3 and 3.2.4 is actually dictated by the requirement that the four boundary conditions associated with $\theta = 0$ (*viz.*, continuity of tractions and displacements across the bondline) be independent of r.

The eight boundary conditions (the remaining four are associated with the traction free surfaces at $\theta = \pm\pi$) yield eight homogeneous equations in the eight unknowns ($a_\alpha, b_\alpha, c_\alpha$, and $d_\alpha (\alpha = 1, 2)$). Because the equations are homogeneous, a nontrivial solution for the constants exists only if the determinant of the matrix of coefficients for the system of linear equations vanishes. Evaluating this determinant and simplifying, the characteristic equation can be written in the form

$$\cot^2 \lambda_c \pi + \left(\frac{\mu_1(\frac{1}{1+\nu_2}) - \mu_2(\frac{1}{1+\nu_1}) - \frac{1}{2}(\mu_1 - \mu_2)}{\mu_1(\frac{1}{1+\nu_2}) + \mu_2(\frac{1}{1+\nu_1})} \right)^2 = 0. \qquad (3.2.5)$$

Writing $\lambda_c = \lambda_r + i\lambda_j$, substituting this eigenvalue into Eq. 3.2.5, and equating real and imaginary parts yields

$$\frac{(tan^2 \lambda_r \pi + 1) \tanh \lambda_j \pi}{tan^2 \lambda_r \pi + \tanh^2 \lambda_j \pi} = \pm \left(\frac{\mu_1(\frac{1}{1+\nu_2}) - \mu_2(\frac{1}{1+\nu_1}) - \frac{1}{2}(\mu_1 - \mu_2)}{\mu_1(\frac{1}{1+\nu_2}) + \mu_2(\frac{1}{1+\nu_1})} \right) \qquad (3.2.6a)$$

and

$$\frac{\tan \lambda_r \pi (1 - \tanh^2 \lambda_j \pi)}{tan^2 \lambda_r \pi + \tanh^2 \lambda_j \pi} = 0. \qquad (3.2.6b)$$

The latter of these equations is satisfied by $\tan \lambda_r \pi = 0$ and by $\tan \lambda_r \pi = \infty$. Thus two sets of solutions are possible. For $\tan \lambda_r \pi = 0$, Eq. 3.2.6 gives

$$\lambda_r = n + 1, n = 0, 1, 2, ... \qquad (3.2.7a)$$

$$\lambda_j = \pm \frac{1}{\pi} \coth^{-1} \left(\frac{\mu_1(\frac{1}{1+\nu_2}) - \mu_2(\frac{1}{1+\nu_1}) - \frac{1}{2}(\mu_1 - \mu_2)}{\mu_1(\frac{1}{1+\nu_2}) + \mu_2(\frac{1}{1+\nu_1})} \right) \qquad (3.2.7b)$$

and for $\tan \lambda_r \pi = \infty$, Eq. 3.2.6 yields

$$\lambda_r = n + \frac{1}{2}, n = 0, 1, 2, ... \qquad (3.2.8a)$$

$$\lambda_j = \pm \frac{1}{\pi} \tanh^{-1} \left(\frac{\mu_1(\frac{1}{1+\nu_2}) - \mu_2(\frac{1}{1+\nu_1}) - \frac{1}{2}(\mu_1 - \mu_2)}{\mu_1(\frac{1}{1+\nu_2}) + \mu_2(\frac{1}{1+\nu_1})} \right). \qquad (3.2.8b)$$

It is important to note that the eigenvalues listed above for both sets of solutions reflect the fact that bounded displacements at the crack tip and bounded strain energy in finite regions about the crack tip require $\Re e\{\lambda_c\} > 0$. Also, the proper interpretation of these results requires that the two sets of eigenvalues be intertwined to form the complete solution to this problem.

3.3 Discussion of the Williams Solution

The singular behavior of the stresses at the crack tip can now be characterized. From Eq. 3.2.3, the stresses behave as

$$\sigma \sim r^{\lambda_c - 1} \sim r^{(\lambda_r - 1) + i\lambda_j}. \tag{3.3.1}$$

For the minimum eigenvalue, *i.e.*, the one with the smallest real part, it is seen that the stresses behave according to (see Eqs. 3.2.7 and 3.2.8)

$$\sigma \sim r^{(-\frac{1}{2} + i\lambda_j)} \sim \frac{1}{\sqrt{r}} r^{i\lambda_j} \sim \frac{1}{\sqrt{r}} \begin{pmatrix} \sin \\ \cos \end{pmatrix} (\lambda_j \log r), \tag{3.3.2}$$

which is of an oscillating character with its maximum modulus determined by $r^{-1/2}$. It is thus observed that the order of the stress singularity at the crack tip ($O(r^{-1/2})$) is the same for the bimaterial problem as it is for the homogeneous case.

For this same minimum eigenvalue, *viz.* $\lambda_c = \frac{1}{2} + i\lambda_j$, the displacements are also seen to exhibit oscillatory behavior (see Eq. 3.2.4):

$$u \sim r^{\lambda_c} \sim r^{\frac{1}{2} + i\lambda_j} \sim \sqrt{r} \begin{pmatrix} \sin \\ \cos \end{pmatrix} (\lambda_j \log r). \tag{3.3.3}$$

Moreover, it can be shown that the displacement oscillations result in predictions of interpenetration of the crack faces in a region (usually small) near the tip of the crack (see for example Williams (1959) and Rice (1988)). On physical grounds, it is conceded that the solutions developed above must be wrong in detail on the scale of the contact zone. However, it is argued that these solutions nevertheless provide a proper characterizing parameter for the near-tip state in typical circumstances when that zone size is much smaller than the crack length. This characterizing parameter is a complex stress intensity factor $K = K_1 + iK_2$, in which local (near-tip) tensile and shear effects are intrinsically inseparable into analogues of classical mode I and mode II conditions.

3.4 The Complex Stress Intensity Factor

Adopting the notation and normalizations introduced by Hutchinson, Mear and Rice (1987) and Rice (1988), the local crack tip stress field for the semi-infinite interface crack of Fig. 3.1 can be written in the form

$$\sigma_{\alpha\beta} = \Re e[K(2\pi r)^{-1/2}\left(\frac{r}{l}\right)^{i\epsilon}\tilde{\sigma}_{\alpha\beta}(\theta)], \tag{3.4.1}$$

where r and θ are planar-polar coordinates centered at the tip of the crack, $i = \sqrt{-1}$, $K = K_1 + iK_2$ is the complex interface stress intensity factor, and

$$\epsilon = \frac{1}{2\pi}\ln\left(\frac{1-\beta}{1+\beta}\right) \tag{3.4.2}$$

may be called the "oscillation index," a quantity that expresses the degree of dissimilarity exhibited by a particular material pair.[1] It is important to note that the angular dependence of the stress field $\tilde{\sigma}_{\alpha\beta}(\theta)$ is, in general, complex.

On the interface ahead of the crack tip ($\theta = 0$), the tractions are given by

$$\sigma_{22} + i\sigma_{12} = \frac{1}{\sqrt{2\pi r}} (K_1 + iK_2) \left(\frac{r}{l}\right)^{i\epsilon}. \tag{3.4.4}$$

It is instructive at this point to compare Eq. 3.4.4 with the analogous expression for the tractions directly ahead of the crack tip in a homogeneous body:

$$\sigma_{22} + i\sigma_{12} = \frac{1}{\sqrt{2\pi r}} (K_I + iK_{II}). \tag{3.4.5}$$

In Eq. 3.4.5, K_I and K_{II} are, respectively, the classical mode I and mode II stress intensity factors. It is important to note that the interface stress intensity factors, K_1 and K_2, are defined such that $K_1 \to K_I$ and $K_2 \to K_{II}$ when the dissimilarity between the two materials vanishes ($\epsilon = 0$). Also note that when $\beta = 0$ and thus $\epsilon = 0$, K_1 measures the normal component of the stresses acting on the interface

---

[1] The parameter β in Eq. 3.4.2 is one of only two non-dimensional parameters upon which solutions to problems of this class depend, as shown by Dundurs (1969). These so-called Dundurs' mismatch parameters are given by

$$\alpha = \frac{\mu_1(\kappa_2 + 1) - \mu_2(\kappa_1 + 1)}{\mu_1(\kappa_2 + 1) + \mu_2(\kappa_1 + 1)} \tag{3.4.3a}$$

and

$$\beta = \frac{\mu_1(\kappa_2 - 1) - \mu_2(\kappa_1 - 1)}{\mu_1(\kappa_2 + 1) + \mu_2(\kappa_1 + 1)}, \tag{3.4.3b}$$

where $\kappa = 3 - 4\nu$ for plane strain and $(3 - \nu)/(1 + \nu)$ for plane stress, μ is the shear modulus, ν is the Poisson ratio, and the subscripts identify the material as indicated in Fig. 3.1. Note that α and β vanish when the dissimilarity between the elastic properties of the two materials vanishes and that these parameters change sign when materials 1 and 2 are interchanged.

and K_2 measures the shear component, regardless of the value of α. However, one must exercise caution to avoid being deceived by the apparently obvious analogies between the mechanics of fracture of homogeneous and of bimaterial solids. In particular, the significance of the $\left(\frac{r}{l}\right)^{i\epsilon}$ term in Eqs. 3.4.1 and 3.4.4 should not be overlooked: Recall that the presence of this term leads to the oscillatory near-tip behavior discussed above[2] $\left(\left(\frac{r}{l}\right)^{i\epsilon} = e^{i\epsilon \log(r/l)} = \cos\left(\epsilon \log\left(\frac{r}{l}\right)\right) + i \sin\left(\epsilon \log\left(\frac{r}{l}\right)\right)\right)$.

From a practical standpoint, the presence of the $\left(\frac{r}{l}\right)^{i\epsilon}$ term requires that a characteristic length l be considered in the context of interfacial fracture mechanics (this parameter is absent from the analogous homogeneous development). In fact, a characterization of the near-tip fields in terms of stress intensity factors is incomplete without specification of this length parameter. That is, the specific values of K_1 and K_2 depend implicitly on the "choice" of l, and thus all three parameters are required to completely characterize the near-tip field.

From a physical standpoint, it is convenient to consider the ratio K_2/K_1 as approximately representing the shear/tension interaction at the crack tip. This interpretation is alluded to in this work to promote an intuitive understanding of the underlying physics of the problem.

---

[2] The reader is referred to Rice (1988) for a more thorough discussion of the "analytical anomalies" inherent in the elastic interface crack problem formulation.

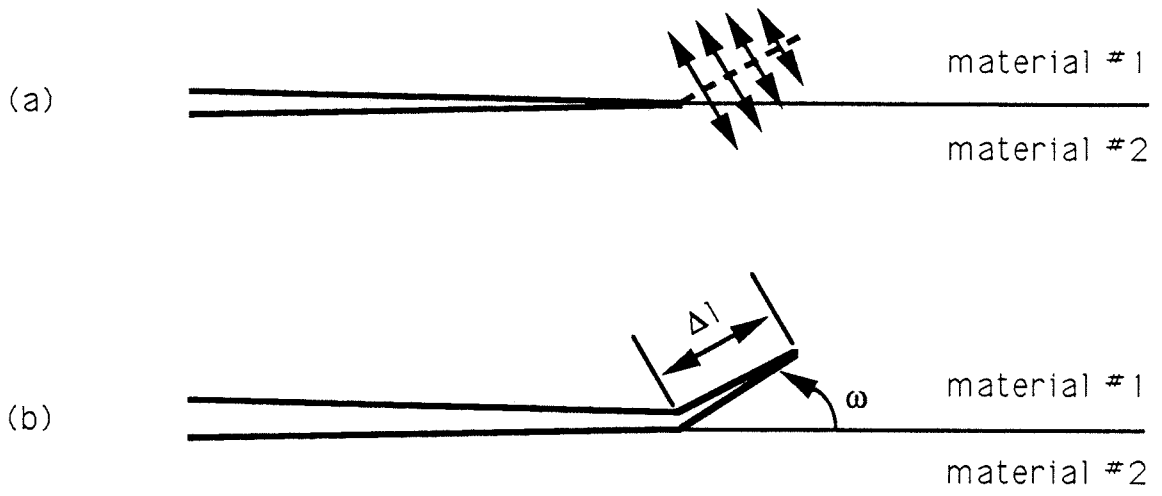

FIG. 3.2 Illustration of the (virtual) radial crack extension sanctioned for the determination of the energy release rate $\mathcal{G}$.

3.5 Kinking of a Crack Out of an Interface

Armed with an understanding of the complex near-tip fields that characterize the interfacial crack problem, it is now conceivable to postulate a criterion that may be exploited to predict the direction of crack propagation for a given bimaterial system subjected to an arbitrary in-plane load. To develop this criterion, it seems prudent to turn to the familiar strain energy release rate concept which has proven so effective in describing the fracture of homogeneous solids.

3.5.1 The Energy Release Rate Concept

The elastic energy release rate of a cracked body, also referred to as the crack driving force, is defined as the energy change in the system due to an incremental growth in crack length Δl. With regard to the interface problem, it is computed as follows:

One allows for a small amount of crack extension Δl to emanate from the current crack tip in an arbitrary, radial direction away from the interface (Fig. 3.2). The angle which the direction of extension makes with respect to the interface is defined as the kink angle ω and is measured positive counterclockwise. Note that a positive value of ω corresponds to an extension into material 1, a negative value implies a kink into material 2, and a zero value refers to propagation along the interface. By computing the work released by the tractions acting along the length of the extension, or equivalently by determining the change in the strain energy stored in the body due to the extension, one can determine the energy release rate $\mathcal{G}$ for these conditions. The energy release rate $\mathcal{G}$ thus represents the energy available for crack advance. It can be expressed mathematically as

$$\mathcal{G} = \lim_{\Delta l \to 0} \frac{1}{2\Delta l} \int_0^{\Delta l} T_i^{(a)} \Delta u_i^{(b)} \, dl = \frac{1}{2} \lim_{\Delta l \to 0} \frac{\Pi^{(b)} - \Pi^{(a)}}{\Delta l}, \tag{3.5.1}$$

where T_i represent the tractions acting along the line of the crack extension prior to its opening, Δu_i represent the displacements through which the tractions are moved, Π represents the elastic strain energy in the body, and the superscripts (a) and (b) refer to the before and after extension states, respectively. The strain energy density Π is given by

$$\Pi = \int_\sigma^\epsilon \sigma_{ij} \, d\epsilon_{ij} = \frac{1}{2} \sigma_{ij} \epsilon_{ij}, \tag{3.5.2}$$

where the last equality holds only for linearly elastic systems.

To determine the critical direction of crack advance for a given loading condition, the maximum energy release rate criterion first mentioned by Erdogan and Sih (1963) is adopted. To apply this criterion, one needs to compute the energy release

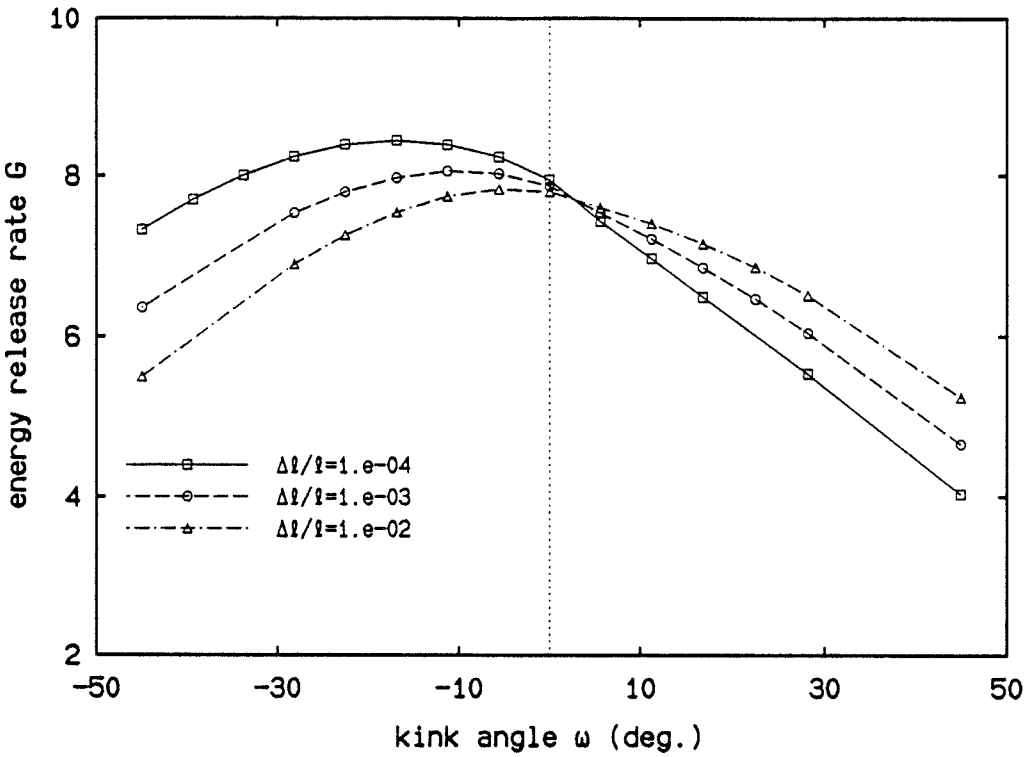

FIG. 3.3 Energy release rate as a function of kink angle for different lengths of kink extension.

rate as a function of the direction of propagation, holding the loading conditions fixed; then, the maximum energy release rate criterion asserts that the crack will propagate in that direction for which the energy released is maximized, provided that the energy released meets or exceeds the energy required for crack advance.

In the case of a homogeneous solid, the energy release rate is independent of the length of the radial extension provided that this extension is "small" relative to the total crack length. Consequently, a unique value of the kink angle for given loading conditions can always be predicted by the maximum energy release rate criterion for cracks in homogeneous bodies. However, Geubelle and Knauss (1991) and Knauss, Geubelle, and Bowen (1991) have demonstrated that, for the linearly

elastic description of the interface problem, the energy release rate depends upon the length of the virtual crack extension. This behavior is illustrated in Fig. 3.3, which contains plots of the energy release rate as a function of kink angle and kink extension for one particular loading. Note that the value of the kink angle ω predicted by the maximum energy release rate criterion (*i.e.*, the value of ω corresponding to the maximum point on the curves) depends, in contrast to the homogeneous case, on the length of the extension utilized to compute $\mathcal{G}$. This situation, that of a non-unique kink angle, is exemplified in Fig. 3.4; this figure exhibits the variation of the energetically most favorable kink angle with the applied loading parameter $\gamma = \tan^{-1}(K_2/K_1)$ and the kink extension Δl.[3] Note that the "master curve" presented in Fig. 3.4 is obtained by shifting the individual curves along the abscissa by an amount $\epsilon \ln(\Delta l/l)$.

The curves presented in Fig. 3.4 are representative of those obtained for a general bimaterial system for which $\beta \neq 0$. (For the special case $\beta = 0$, the non-uniqueness of the energy release rate vanishes and only a single curve is obtained, regardless of the length of the (small) virtual crack extension.) Thus, as noted by Geubelle and Knauss (1991), the maximum energy release rate criterion does not provide a unique value of the kink angle in the general bimaterial case of $\beta \neq 0$; again, as with the determination of the stress intensity factors, a length scale (here the length of the extension) must be introduced in order to make the criterion unique. This characteristic length, referred to as Δl^*, would need to be determined experimentally for a given bimaterial system by computing the horizontal shift of the master curve required to provide a best-fit to the experimental data. Although this characteristic length may be considered a "property" of the bimaterial system,

[3] The occurrence of a non-unique kink angle is not a consequence of the criterion used to deduce this angle. The anomalous behavior discussed above also arises in problem formulations that utilize maximum strain or maximum stress criteria of the Erdogan/Sih type.

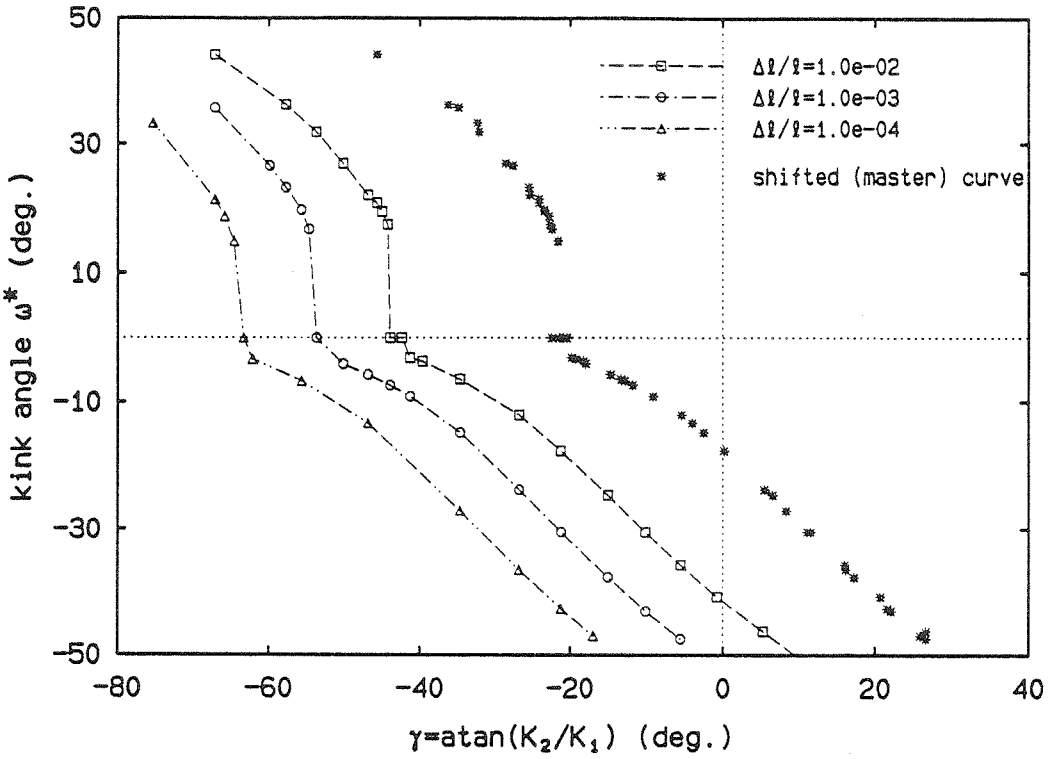

FIG. 3.4 Kink angle (determined by the maximum energy release rate criterion) as a function of mixed-mode loading $\gamma = \tan^{-1}(K_2/K_1)$ for different lengths of kink extension Δl.

its physical significance is unclear at this time. (It may, for example, correspond to a characteristic flaw size or the size of a damage zone.) It is emphasized that the length scale Δl^* is not a part of the fracture model, but rather a "retrofit parameter" required to fit the linearized analysis to the experimental data.

In the following section, the non-unique nature of the energy release rate is circumvented in order to provide heuristic insight into the role of fracture toughness on the expected crack kinking behavior.

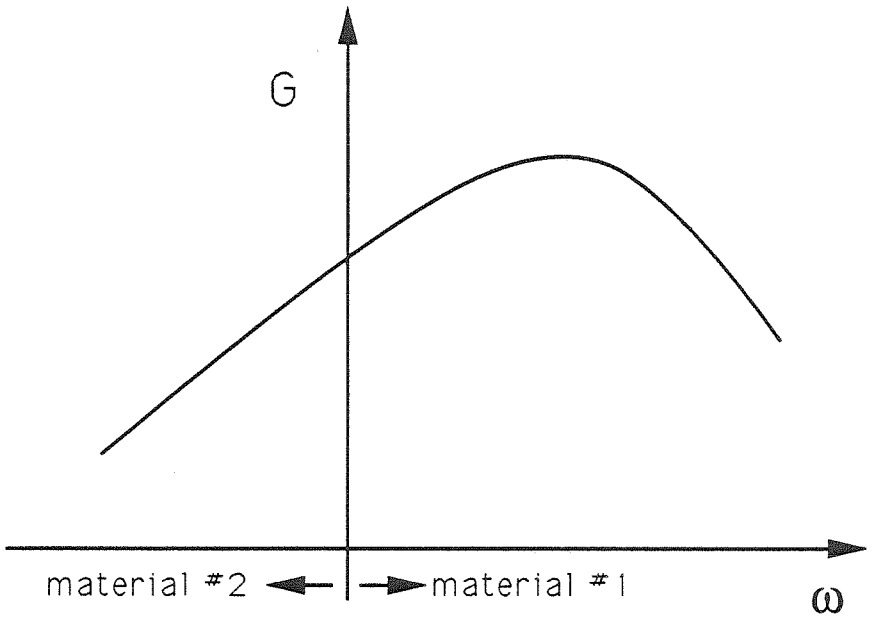

FIG. 3.5 Schematic variation of $\mathcal{G}$ for a given loading.

3.5.2 The Role of Fracture Toughness

The variation of the energy release rate $\mathcal{G}$ with kink angle ω for an arbitrary loading condition is shown schematically in Fig. 3.5.[4] In order to determine the direction of crack advance, the computed energy release rates must be compared with the energies required for propagation (fracture toughnesses) into either material or along the interface. For this discussion, the fracture toughnesses of materials 1 and 2 shall be denoted as $\mathcal{G}_{1c}$ and $\mathcal{G}_{2c}$, and that of the interface as $\mathcal{G}_{0c}$. In order to exemplify the role of material toughness on the predicted fracture behavior, three limiting cases shall be discussed below.

Consider first a situation in which the three fracture toughnesses are identical, *i.e.*, $\mathcal{G}_{1c} = \mathcal{G}_{2c} = \mathcal{G}_{0c}$. By modifying Fig. 3.5 to incorporate this information,

[4] The reader is reminded that the non-unique nature of the energy release rate is circumvented here for the sake of clarity of presentation.

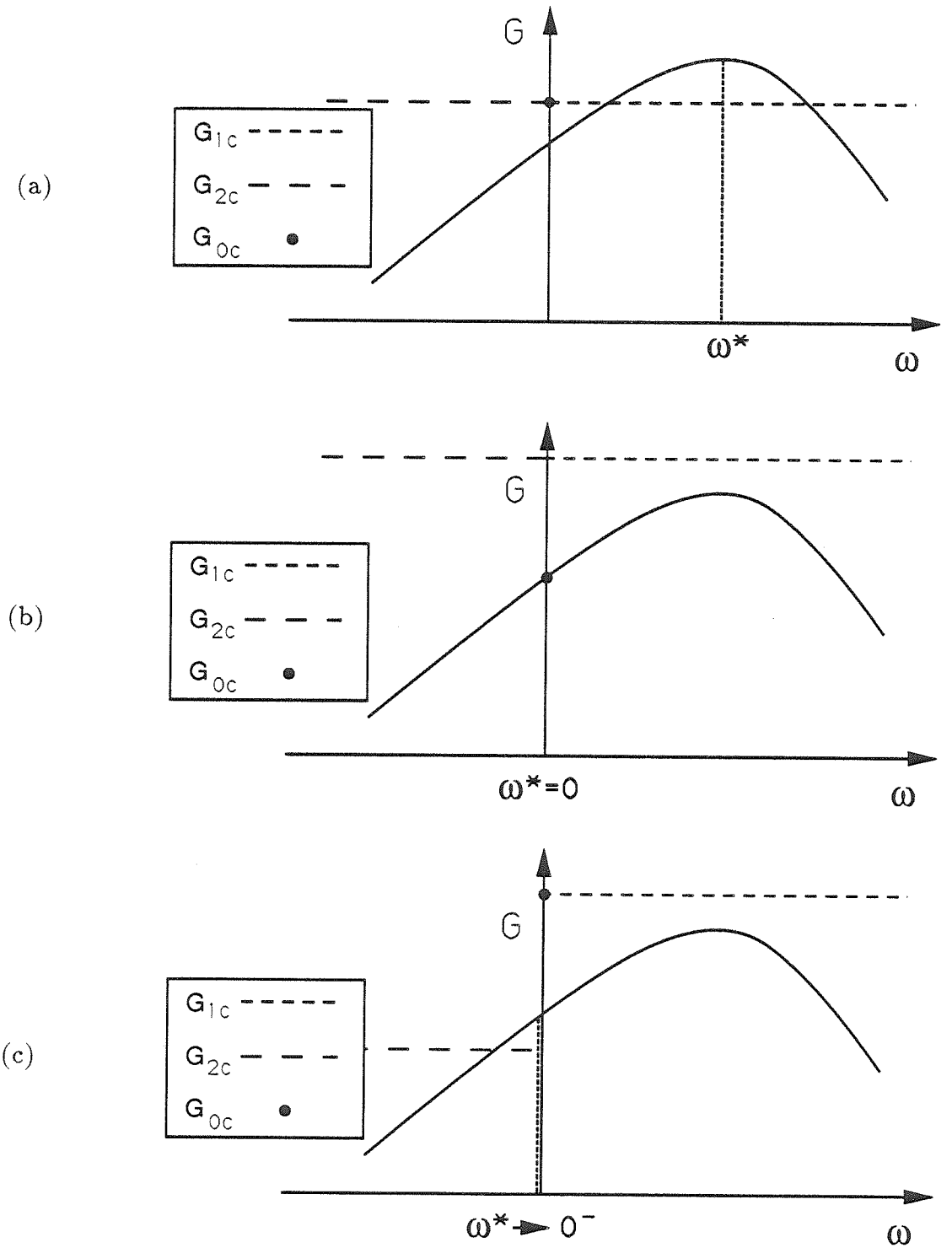

FIG. 3.6 The influence of fracture toughness on crack propagation behavior.

Fig. 3.6a can be constructed. Note that although the three fracture toughnesses are identical, they are appropriately differentiated in Fig. 3.6a according to the value of ω. Although the energy available for crack advance exceeds that which is required for a finite range of kink angles, energy release is maximized by crack advance into material 1 at the angle ω^*; consequently, the maximum energy release rate criterion predicts that the crack will propagate in this direction.

As a second illustration of the influence of material strength on the kinking behavior, consider the case of a very weak interfacial bond between two solids of comparable toughness. This situation can be represented by the plot in Fig. 3.6b. Although the maximum energy release rate corresponds to a kink into material 1, the comparatively high strength of this material precludes this failure mode. Instead, the solid will fracture along the (weak) interface ($\omega = 0$).

As a final illustration of the influence of fracture toughness on the ultimate kinking behavior of the bimaterial solid, consider the case of a strong (tough) bond between a very tough solid and a very weak solid. This situation is depicted in Fig. 3.6c. In this case, the energy available for crack advance exceeds that which is required for a small range of negative kink angles. Since the maximum energy release rate criterion maintains that crack advance will occur in that direction for which the energy released is maximized, the crack will propagate into the weak material (material 2) at a vanishingly small angle ($\omega \rightarrow 0^-$). Note that it may be difficult in practice to distinguish this type of crack trajectory from that suggested by Fig. 3.6b.

The energy release rate curves of Figs. 3.5 and 3.6 correspond to a single arbitrary loading condition γ. In order to construct a comprehensive plot of kink angle ω versus loading angle γ, one needs to consolidate the pertinent information

from a series of graphs, each similar to the plot shown in Fig. 3.5, that extends over the gamut of loading conditions. For the purpose of this heuristic exposition, the "pertinent" information to be garnered from each loading condition includes the value of the maximum energy release rate and its accompanying (energetically most favorable) kink angle, and the value of the energy release rate corresponding to crack advance along the interface.

The energy release rates corresponding to propagation along the interface, into material 1, and into material 2 are denoted by $\mathcal{G}_0$, $\mathcal{G}_1$, and $\mathcal{G}_2$, respectively. After compiling the aforementioned information for the gamut of loading conditions, one can construct plots of the ratios $\mathcal{G}_1/\mathcal{G}_0$ and $\mathcal{G}_2/\mathcal{G}_0$ as functions of γ, as shown in the top graph of Fig. 3.7. Recall that these curves represent the energies available for crack advance. To determine the direction of propagation, these curves must be compared with those representing the energies required for propagation into either material or along the interface. For simplicity, these required energies shall be assumed independent of the character of the local stress field. Hence, the fracture toughness ratios $\mathcal{G}_{1c}/\mathcal{G}_{0c}$ and $\mathcal{G}_{2c}/\mathcal{G}_{0c}$ shall plot as horizontal lines, as indicated in Fig. 3.7. Two limiting cases shall be discussed below.

Consider first the case of a weak interface between two materials of comparable toughness. This situation dictates that the ratios $\mathcal{G}_{1c}/\mathcal{G}_{0c}$ and $\mathcal{G}_{2c}/\mathcal{G}_{0c}$ shall be relatively large, and it may not be possible to satisfy the energy requirements for fracture into either of the two materials; consequently, fracture must occur by crack advance along the interface. This situation is represented in Fig. 3.7 as the horizontal line denoted by the letter "A."

Next consider the case in which the interface is as tough as either of the two adherends. For this scenario, the fracture toughness ratios $\mathcal{G}_{1c}/\mathcal{G}_{0c}$ and $\mathcal{G}_{2c}/\mathcal{G}_{0c}$

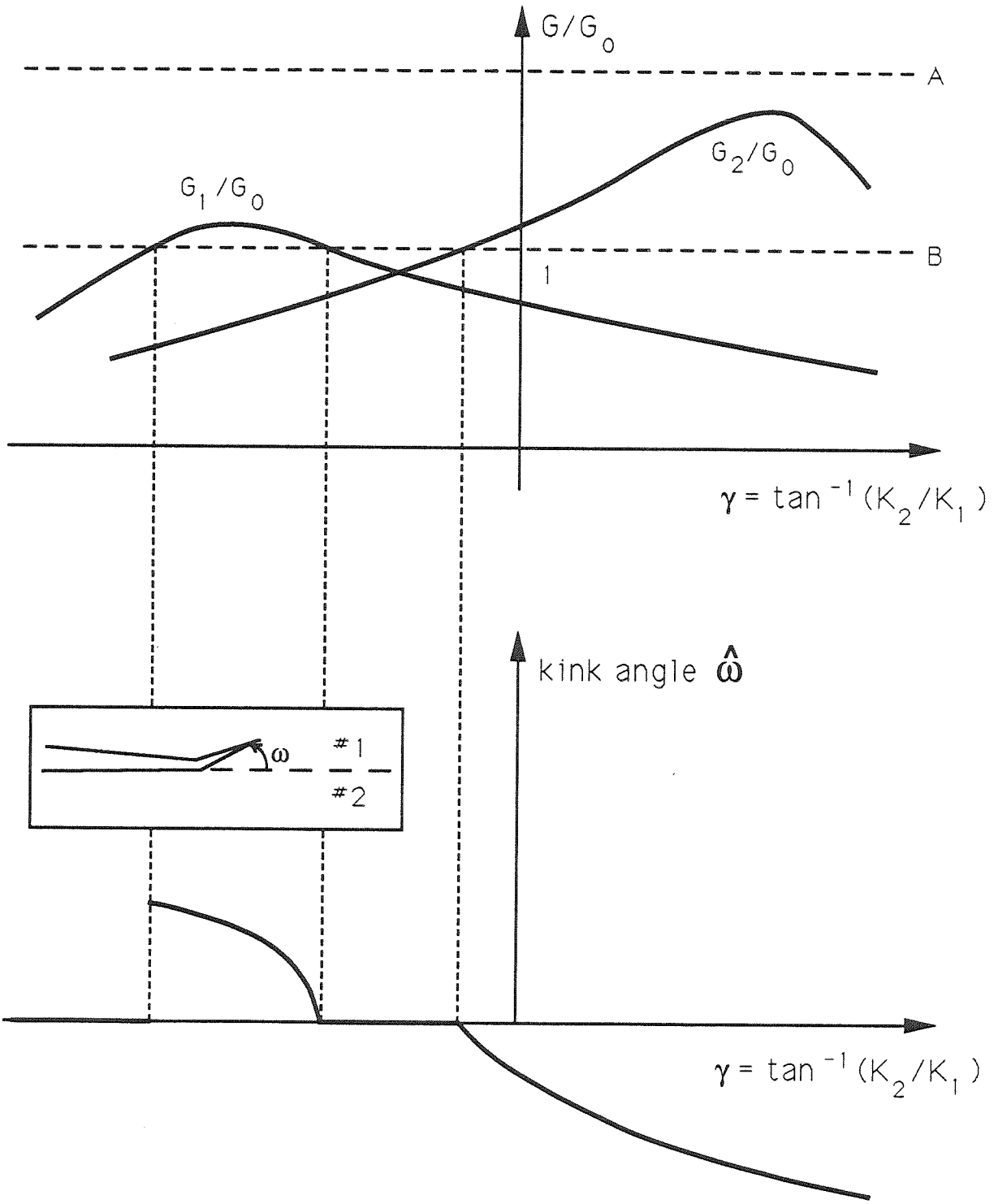

FIG. 3.7 Estimates of crack kinking based on relative energy release rates and fracture toughnesses.

are on the order of unity, as represented by the line identified by the letter "B" in Fig. 3.7. Energy considerations suggest crack growth into material 1 when $\mathcal{G}_1/\mathcal{G}_0$ exceeds $\mathcal{G}_{1c}/\mathcal{G}_{0c}$, and into material 2 when $\mathcal{G}_2/\mathcal{G}_0$ exceeds $\mathcal{G}_{2c}/\mathcal{G}_{0c}$; where these conditions are not met, crack advance can only occur along the interface. This analysis thus leads to the kink angle - loading angle curve illustrated schematically in the lower portion of Fig. 3.7.

The plot in the lower portion of Fig. 3.7 represents the most general fracture behavior that can be exhibited by a bimaterial joint: The crack can advance by propagation along the interface or into either of the adjacent materials, depending on nature of the (local) shear/tension interaction acting at the tip of the crack. The observance of such general behavior experimentally is contingent upon the receipt of a "sufficiently tough" bond between the two materials that comprise the bimaterial joint. In the following chapter, the bimaterial specimen designed to exhibit this behavior is discussed.

CHAPTER 4

The Bimaterial Fracture Specimen

4.1 Introduction

As elucidated in the previous chapters, the mechanics of crack propagation at and near a planar interface between two (visco)elastic materials is a complex problem. In order to assess analytical predictions and numerical results, it is necessary to perform an ample amount of bona fide experimental work.

Prerequisite to the experimental investigation is the design and manufacture of appropriate bimaterial specimens. These fracture specimens should be amenable to both numerical analysis and mechanical preparation techniques. Ideally, these specimens should have a well-defined, planar interface and perfect bonding between the two materials. Furthermore, the stiffnesses of the constituent materials should differ significantly in order to accentuate the non-homogeneity across the bondline. Finally, it is necessary to fully characterize the material behavior of each of the two constituents in order to ultimately analyze the bimaterial specimens.

"Solithane 113" is the trade name for a polyurethane elastomer manufactured by Morton Thiokol, Inc., and it serves as the model material in this study. It is synthesized by mixing a "urethane resin" (isocyanate terminated polyol) and a "catalyst" (ricinus oil) at 65 C, and then curing the resulting mixture according

to a curing cycle that climaxes with a 90 minute tarry at 150 C. By varying the ratio of resin to curative, Knauss and Mueller (1967) and Mazor and Bowen (1989, 1990) have shown that it is possible to cast elastomers that exhibit a considerable range of mechanical behavior. Thus it is possible to prepare bimaterial specimens that are comprised of two different compositions of the same base material. This situation helps to promote strong chemical bonding across the interface between the two adherends.

Previous interfacial fracture work carried out at GALCIT by Knauss (1988) involved Solithane 65/35 and Solithane 50/50.[1] One initial intention was to continue and further this research, using the same compositions of Solithane, and exploiting the "known" mechanical properties of these materials (Knauss and Mueller, 1967). However, in the course of attempting to duplicate previous results, it was found that the relative stiffnesses of the two different compositions employed changed with time when left exposed to the laboratory environment. This apparent aging behavior necessitated a separate study to fully characterize the mechanical behavior and aging properties of a broad spectrum of compositions of Solithane. The results of that study (Mazor and Bowen, 1990) dictated the optimal choice of compositions for bimaterial specimens manufactured from Solithane, *viz.* 55/45 and 45/55. This chapter discusses the process developed to manufacture the bimaterial fracture specimens utilized in the present experimental work.

---

[1] The "number/number" notation is used in reference to Solithane to denote the "weight percent resin-to-curative ratio"; *e.g.*, the 65/35 composition is 65% resin and 35% curative, by weight.

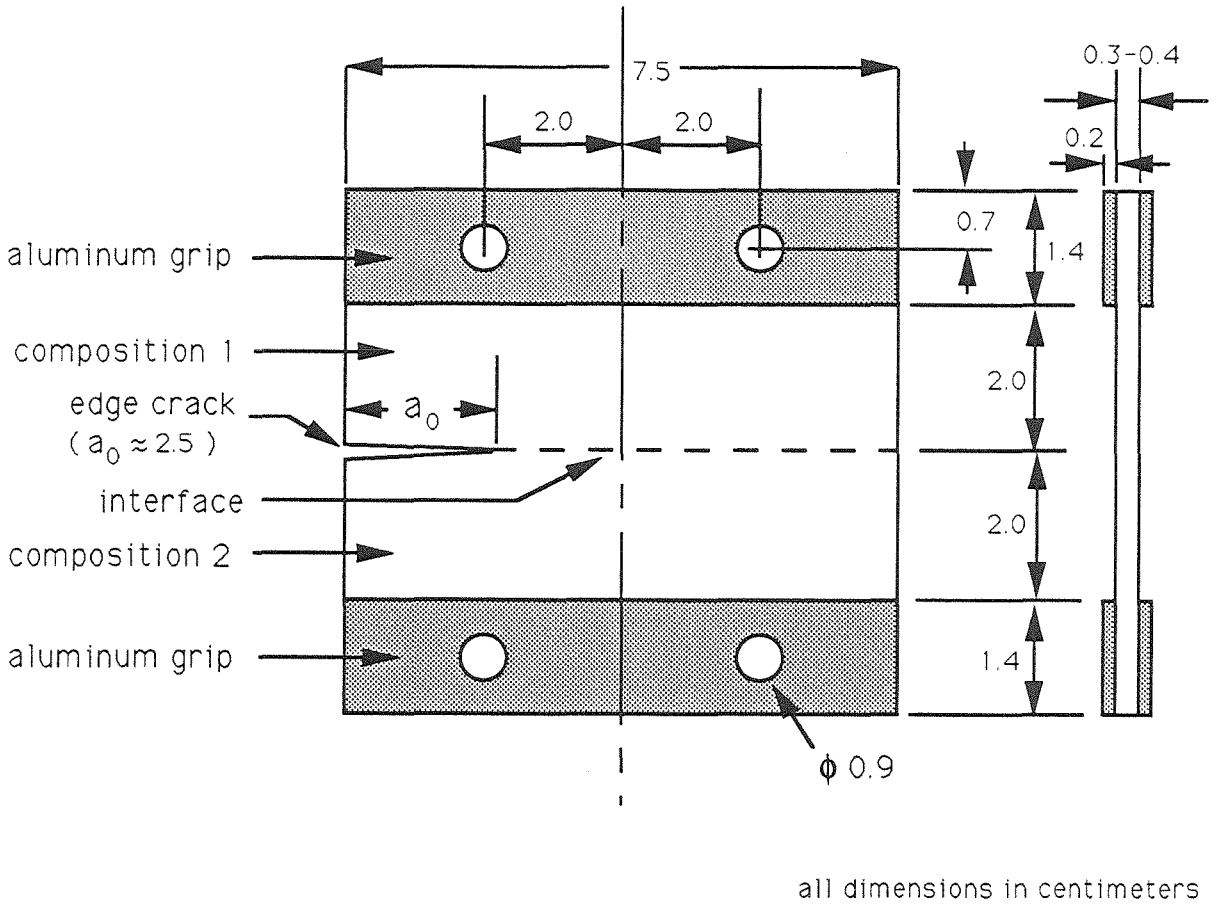

FIG. 4.1 Geometry of the bimaterial fracture specimen.

4.2 Geometry of the Bimaterial Fracture Specimen

The question of a suitable bimaterial test geometry was first addressed by Mazor and Bowen (1989). With Solithane serving as an initial model material, several geometries and manufacturing techniques were discussed and tested, and a bimaterial "thick sheet" specimen was recommended for the ultimate bimaterial fracture analysis. Improved manufacturing techniques have contributed to the evolution of this specimen into a thinner derivative, a plane stress test specimen, which has been utilized for this research effort. This type of fracture specimen is illustrated in Fig. 4.1, and a photograph of an actual specimen is presented in Fig. 4.2. This specimen is a logical bimaterial extension of the familiar homogeneous rectangular

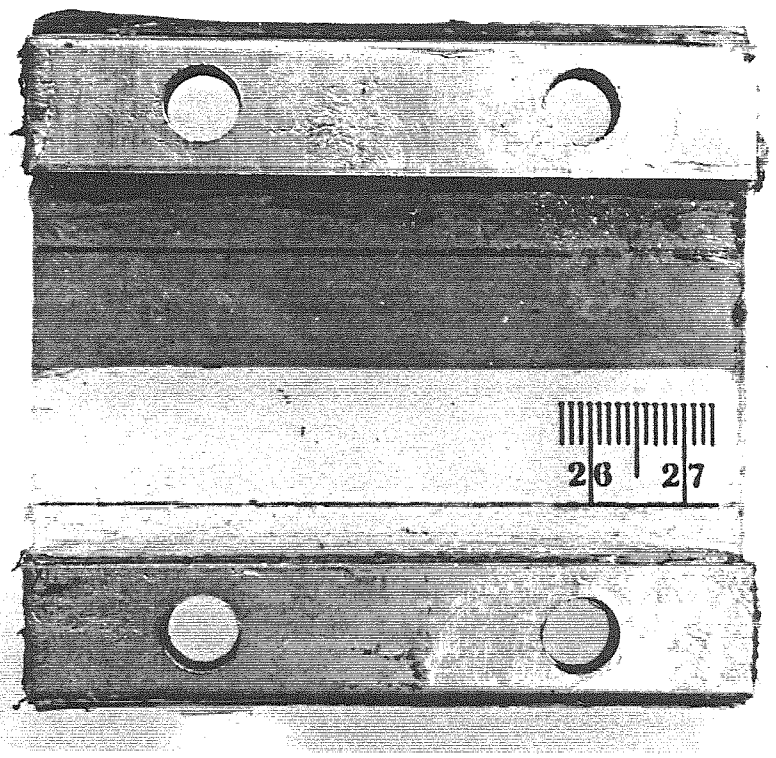

FIG. 4.2 Photograph of a bimaterial fracture specimen.

sheet specimen with an edge crack. It should be noted, however, that its dimensions have been designed to provide a practical approximation to the semi-infinite strip model, for which the stress intensity factor is independent of crack length. (The merit of this geometry has been validated by Bowen (1991).)

Of primary concern in bimaterial specimens is the strength of the bond between the materials, and the integrity of what should ideally be a planar interface between them. Mazor and Bowen (1989) have demonstrated an exceptional procedure for fabricating Solithane bimaterial specimens that involves partially curing, in "block" form, the first composition before introducing the second, and then allowing the composite, bi-level brick to co-cure completely; the ultimate fracture specimen is

cut or otherwise machined from the fully cured bimaterial brick. The specimens used in this study were manufactured according to this procedure, which is outlined below.

4.3 Specimen Preparation

The two compositions that comprise the bimaterial specimen are 55/45 and 45/55. Although each composition exhibits a different shade of pale amber, a blue dye[2] is added to the 55/45 composition in order to more clearly define the interface that exists between them. This dye is soluble in the curing agent, but the process takes several days to reach completion at room temperature. The dyed mixture is prepared as follows: enough of the powdered dye is mixed into several hundred grams of curing agent in order to net a solution containing 0.1% dye by weight. The resulting mixture is a pale blue solution with a suspension of tiny, dark blue particles. After about two days, the dye is seen to completely dissolve and the solution achieves a uniform, deep blue color.

The bimaterial block is cast in two steps. First, the 55/45 composition (which shall be referred to as "material 1" in subsequent chapters) is prepared: 308 grams of resin are added to 140 grams of virgin curing agent and 112 grams of dyed curing agent in a 1000 ml Erlenmeyer flask. The highly viscous resin is added to the less viscous curing agent in order to facilitate the mixing of the two substances; admitting the constituents in the reverse order substantially impedes the mixing process. The resulting Solithane mixture is 0.02% dye by weight and provides a satisfactory color tone for the purposes of this research.

---

[2] Aldrich Chemical Company, Acid Blue 25.

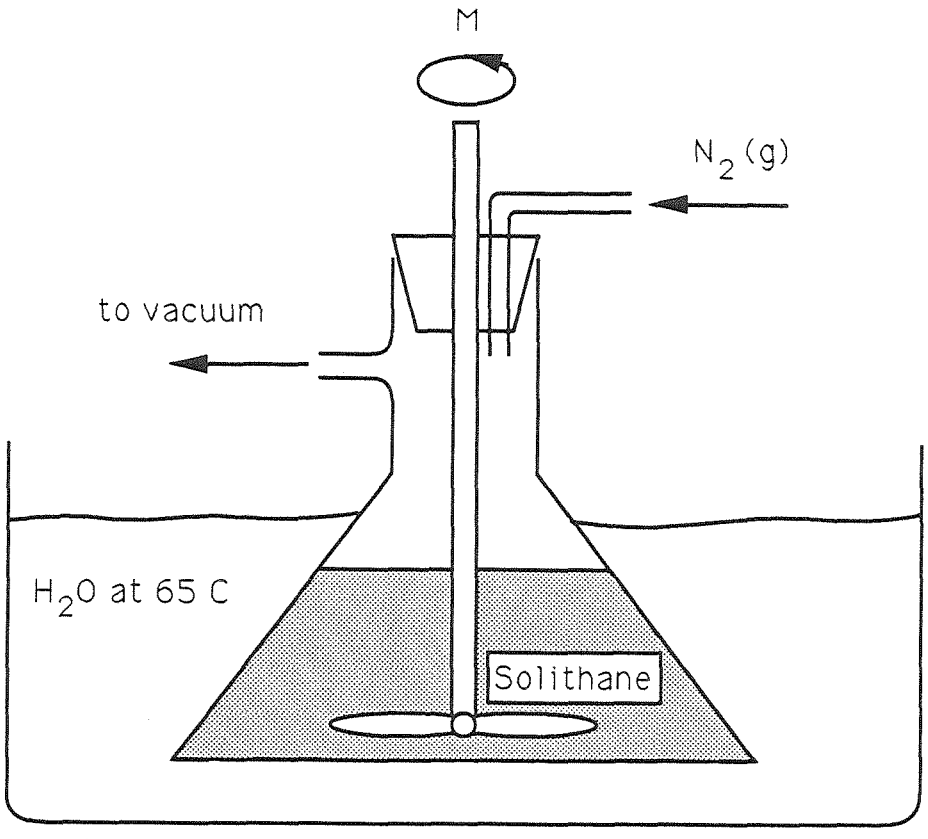

FIG. 4.3 Apparatus for mixing Solithane.

The flask is maintained at 65 C by partial immersion in a controlled water bath of this temperature, and the contents are mixed under vacuum for ten minutes. Periodically throughout the mixing process, the vacuum is relaxed and nitrogen gas is briefly introduced in order to release O_2 and N_2 bubbles that develop inside the Solithane during the reaction (Fig. 4.3).

After completion of the mixing phase, enough Solithane is transferred into the lower half of a two-piece mold to nearly fill it. This mold has been maintained at 65 C overnight to ensure a uniform temperature distribution throughout. It has also been treated with a TFE (trichlorofluoroethane) release agent[3] in order to

[3] Miller-Stephenson Chemical Company, Inc., TFE Release Agent/Dry Lubricant, MS-122/CO2.

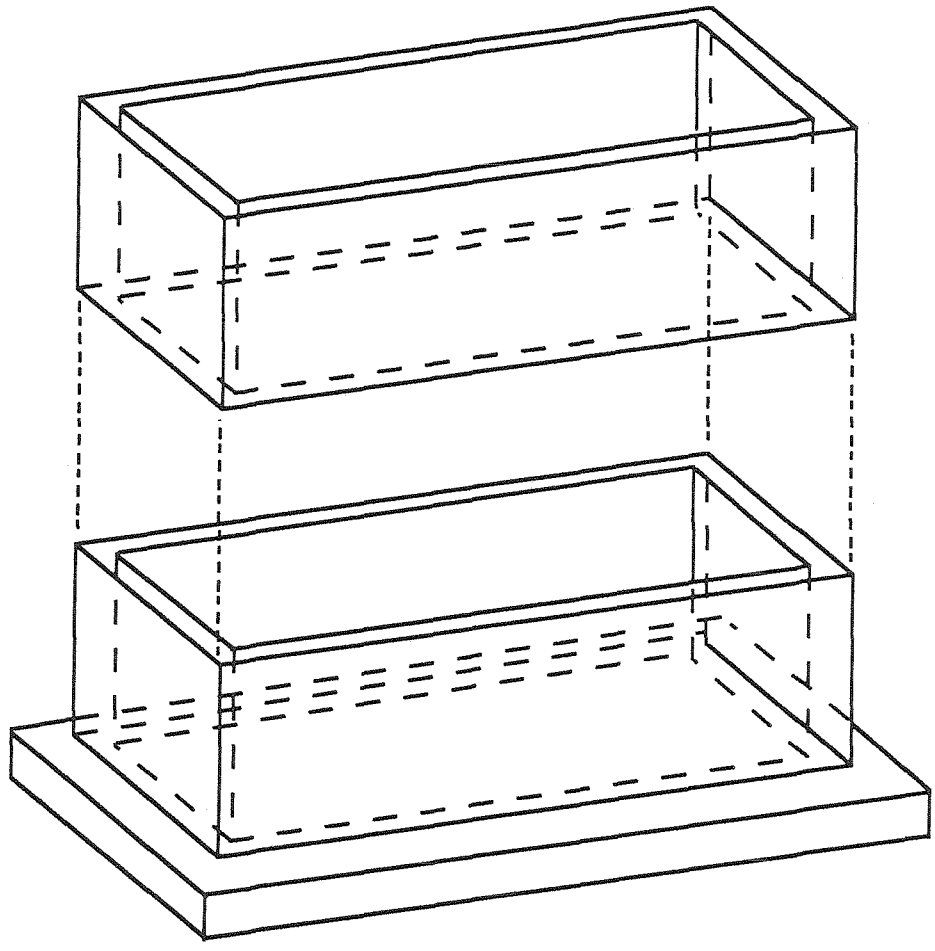

FIG. 4.4 Exploded view of the two-piece mold.

facilitate the eventual removal of the cured sample. The fully assembled mold is an aluminum parallelepiped with internal dimensions of 16.5 cm x 7.5 cm x 12.0 cm, the last dimension denoting the overall height (Fig. 4.4). The upper and lower halves are not fastened together until just prior to the addition of the second composition of Solithane. The lower half has a depth of only 4.0 cm, and since it is nearly completely filled with 55/45, the upper, free surface of this composition of Solithane is readily accessible while the mold is disassembled. This free surface provides the site for the interface, and the importance of easy access to it will become apparent later.

The mold and its batch of 55/45 are then heated to 80 C and held at this temperature until the onset of "gelling," usually 30 to 45 minutes, depending on the lot of Solithane used. This period is the most critical of the entire curing cycle: If the material is allowed to cure too much, chemical bonding across the interface is diminished, and the resulting interface will possess poor bond strength; if, on the other hand, the curing process is not allowed to proceed far enough, the materials will mix upon the addition of the 45/55, thus precluding the receipt of a planar interface.

The transition from not enough to too much "gelling" is rather sudden and cannot be very accurately predicted. Hence the surface of the Solithane is frequently examined for the desired extent of "gelling": When the material is ready, a slender wooden stick touched to its surface will become stuck to it. By raising the stick, a conical peak of Solithane can be made to rise from the surface, typically capable of reaching a height of one centimeter before the Solithane frees itself from the wooden probe. When the Solithane releases from the stick, it slowly makes its way back to the bulk of the sample and the surface resumes its previous, flat form, as if unaffected by the recent course of events.

Once the first batch of Solithane has attained the desired consistency, the mold is removed from the oven and maintained at room temperature. Then, the 45/55 composition is prepared according to a procedure analogous to that used for the 55/45, with the exception of the use of dye: 252 grams of resin are added to 308 grams of virgin curing agent and the solution is mixed, at 65 C and under vacuum, for ten minutes. The natural color of this layer is preserved in order to differentiate between the two compositions in the final specimen.

As the second composition is mixing, the parallelepiped mold and the partially

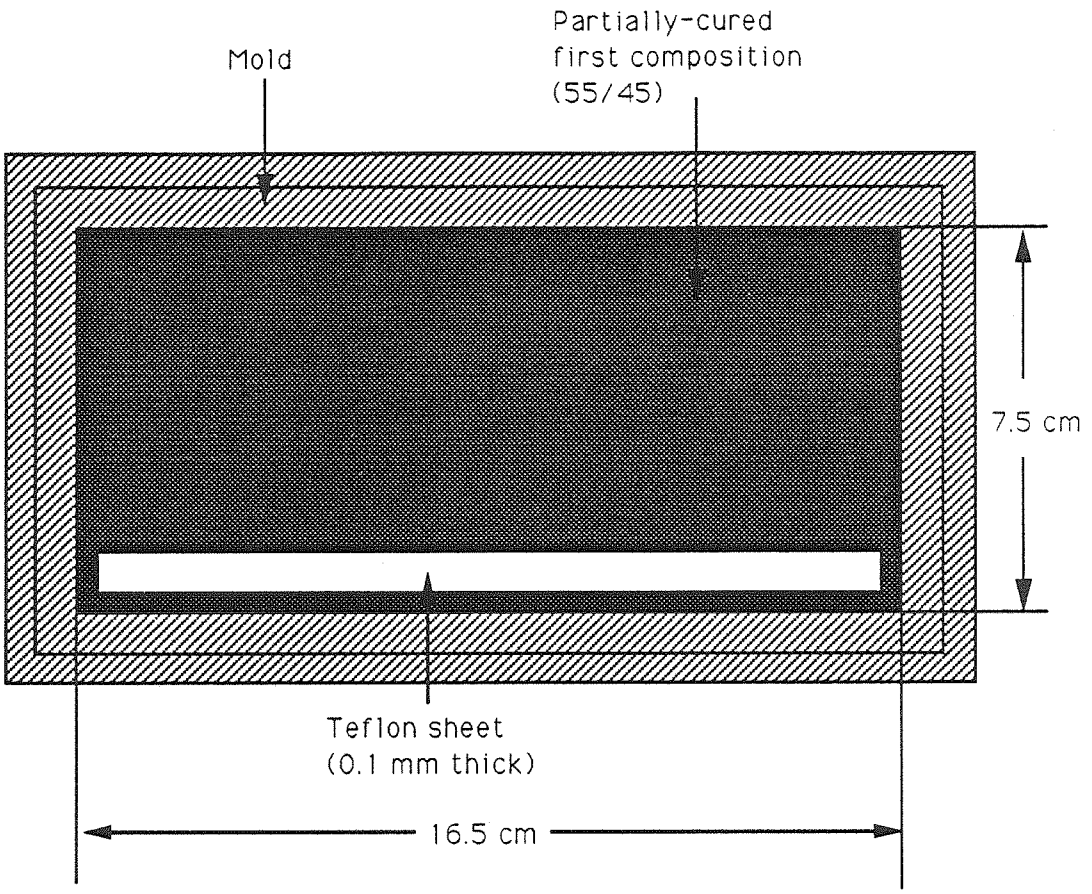

FIG. 4.5 Lower half of mold with Solithane and teflon tape, top view.

cured first layer are readied for the addition of the second composition. A thin sheet of teflon (15.5 cm x 1.2 cm x 0.01 cm) is placed along and parallel to one of the longer edges of the free surface of the partially cured 55/45. It is positioned such that there is 0.5 cm between the inner wall of the mold and the closest lengthwise edge of the teflon (Fig. 4.5). This separation is also maintained along each of the two edges perpendicular to the lengthwise direction of the teflon. This technique avoids sample preparation complications associated with the more pronounced non-planarity of the surface of the partially cured first layer near the walls of the mold. (The nonplanarity exhibited by these near-boundary regions is a consequence of predominating surface tension effects there.)

Since the teflon strip will define the interfacial crack, its integrity and placement are critical. To assure its integrity, the teflon is passively "ironed" for several hours prior to sample preparation: It is cut to size and then maintained overnight at 80 C in between two smooth, heavy steel plates. This operation helps to ensure planarity of the teflon and retards the natural tendency of the thin sheet to curl while it is being handled.

The placement of the teflon strip on the exposed 55/45 is the step that necessitates a two-piece mold - it is much more convenient and efficient to place the teflon on top of a readily accessible surface than onto a surface that lies relatively deep within a narrow mold. After the teflon has been put in place with tweezers, it is carefully "brushed" with the tips of the tweezers in order to free air bubbles that may be trapped between the lower surface of the teflon and the Solithane 55/45. Finally, the upper half of the mold is securely fastened to the lower half.

Once the mixing cycle for the 45/55 has been completed (10 minutes at 65 C), this composition is introduced into the fully-assembled mold on top of the partially cured 55/45 and the teflon sheet. The teflon prevents the two compositions from coming into contact in the region it occupies and hence provides an area where no bonding across the interface occurs. This region, located exactly at the interface between the two materials, defines a "crack" in the final specimens. To obtain the desired edge crack, the 0.5 cm ligament of material behind the teflon in the fully cured, cut sheets will be mechanically cut prior to performing any fracture tests.

Next, the two compositions are allowed to fully cure together in the mold, according to the following heating cycle: 60 minutes at 80 C, followed by 30 minutes at 90 C, 15 minutes at 110 C, 15 minutes at 130 C, and finally 90 minutes at 150 C. A typical temperature-history curve of the complete curing cycle is shown in Fig. 4.6.

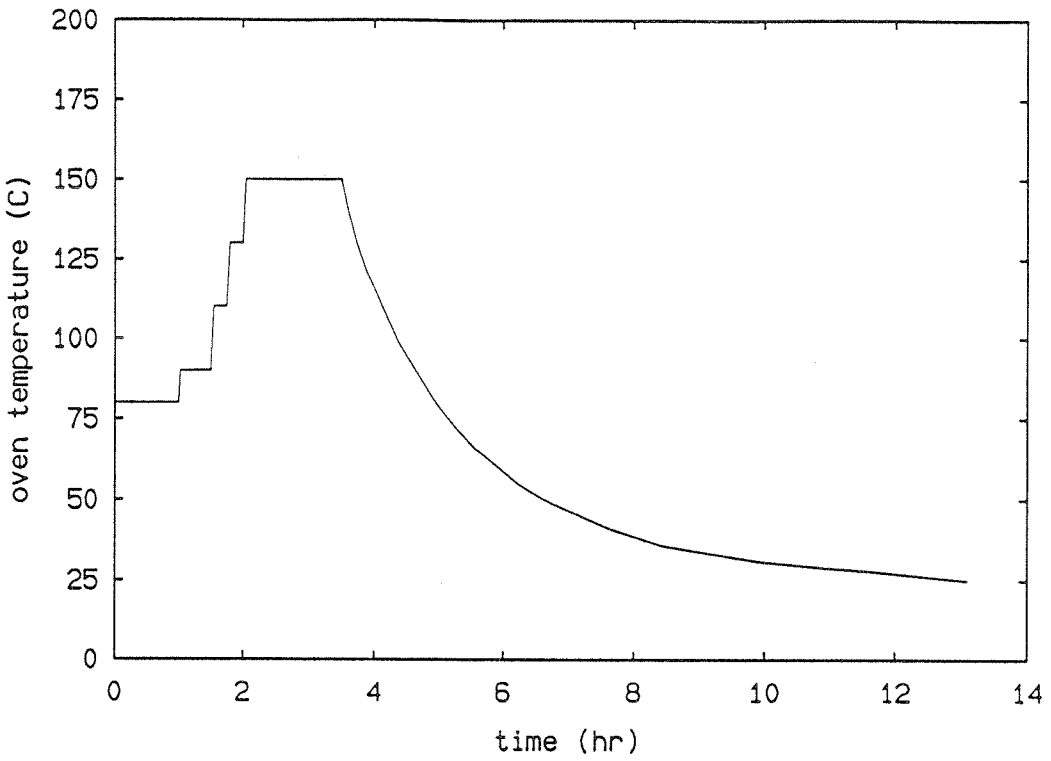

FIG. 4.6 The temperature cycle for co-curing the bimaterial Solithane block.

The first step of this curing cycle is designed to eliminate any initial temperature gradients that may exist within the bulk of the sample. The next three steps are needed to keep gradients due to heating at an acceptable level as the Solithane is brought to its final curing temperature of 150 C. At the completion of the curing cycle, the oven is shut off and the sample is allowed to cool inside the closed oven overnight. This very slow cooling of the Solithane brick minimizes temperature gradients and hence prevents cracks from appearing in the bulk of the cured and highly volume confined elastomer as it is cooled.

Once the mold has cooled to ambient temperature, it is dismantled and the elastomer removed. The fully cured Solithane block is 16.5 cm x 7.5 cm x 8.0 cm, the last dimension denoting its height. The contrast in the colors of the compositions

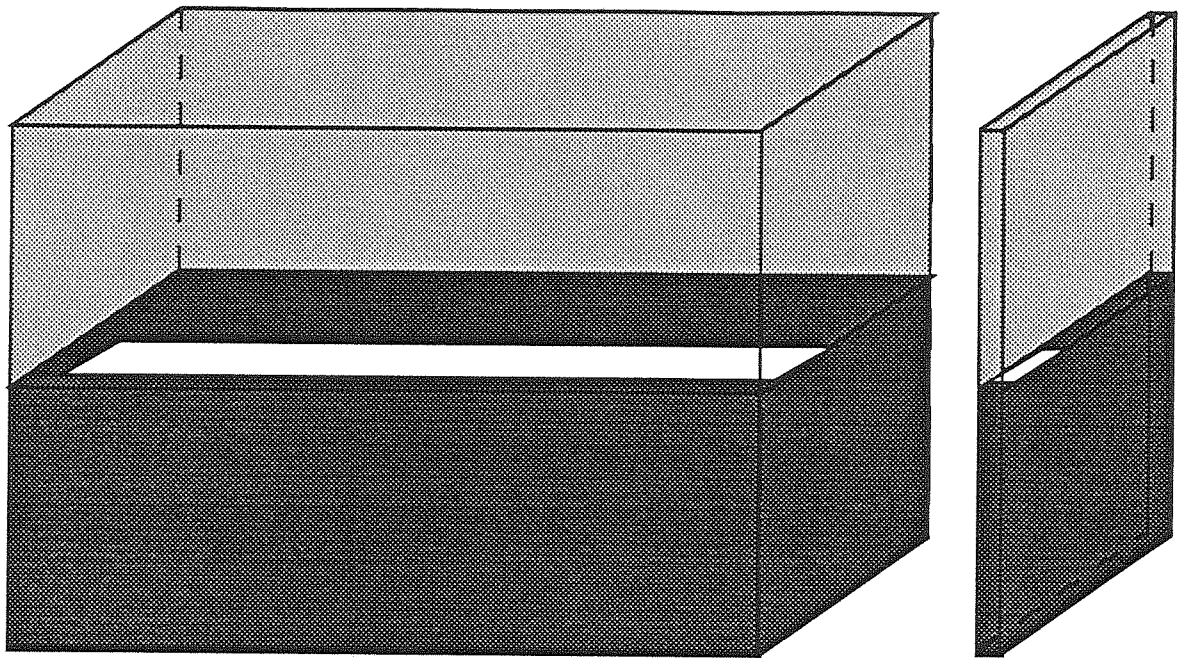

FIG. 4.7 Cutting the bimaterial block.

clearly delineates the interface between them, and the transparency of the 45/55 layer permits observation of the internal teflon strip.

A band saw is used to cut thin slices or sheets ($\approx 0.3\,\text{cm}$) from the block sample with the aid of a specially-designed support apparatus that helps maintain specimen alignment and improves the quality of the parallel cuts. The cuts are made perpendicular to both the interface and the lengthwise direction of the solid block (Fig. 4.7). Approximately 30-35 specimens suitable for testing can be obtained from each block. It is noted that the two specimens that had bordered along opposite walls of the mold are discarded because of the surface tension-induced curvature of their interfaces.

To reduce the surface roughness and fine ridges introduced by the band saw, the thin sheets are "polished" with wet sandpaper. However, the rubber-like consistency

of the Solithane prevents it from achieving a clear, glass-like finish, regardless of the extent of polishing. Hence, to restore a transparent appearance to the Solithane, the sheets are coated with a fine layer of liquid Solithane that is allowed to cure overnight at 65 C. This coating, less than 0.01 cm thick, restores the glassy appearance to the Solithane samples by filling in the fine cracks and scratches introduced during machining and polishing of the sheets.

The Solithane used for this cosmetic coating is 40/60, a composition chosen for its low viscosity. The sheets are individually dipped into a 40/60 bath and then suspended in an oven maintained at 65 C. The slow curing treatment allows excess 40/60 to run off the samples before a very thin adhering layer finally cures. Furthermore, the low temperature involved does not affect the mechanical properties of the previously cured Solithane.

When the coating has dried, or cured, thin aluminum loading grips are bonded with an RTV silicone rubber adhesive[4] to the specimen. On each face of the specimen, these grips are aligned parallel to and symmetrically about the interface such that the test specimen has a "height" of 4.0 cm (Fig. 4.1). Next, the holes required for pins used to load the specimen during testing are drilled through the grips and the underlying Solithane. Proper alignment of these holes is assured by use of a custom-built jig. It should be noted that the holes are drilled after the aluminum grips are in place because the aluminum is needed to lend support to the rubbery Solithane.

Before testing, the 0.5 cm ligament of Solithane behind the crack, which is defined by the teflon strip, is cut with a razor blade. Finally, using the load frame described in the next chapter, the crack is forced to propagate along the interface

[4] General Electric Company, Silicone Products Division, RTV 108.

for $2-3\,\mathrm{mm}$ so that a natural crack tip, located exactly at the interface, is obtained. This procedure eliminates the influence of the teflon sheet on the ultimate geometry of the crack tip and results in a more objective test.[5] At this point, specimen preparation is complete and fracture testing may proceed.

[5] Preliminary experimental work involving similar specimens, but with the as-cast edge of the teflon sheet serving as the crack tip, suggests that the shape of the edge of the teflon, as well as its thickness, has a strong influence on the fracture behavior of the joint: The data scatter in kink angle measurements for a variety of loading conditions was sufficiently large to prevent any definitive conclusions from being drawn.

CHAPTER 5

Experimental Procedure

5.1 Analytical Modelling of the Fracture Specimen

In light of the equilibrium compliance of Solithane (at 25 C, $E^{\infty}_{55/45} = 3.19\,\mathrm{MPa}$ and $E^{\infty}_{45/55} = 1.23\,\mathrm{MPa}$; at 60 C, $E^{\infty}_{55/45} = 3.44\,\mathrm{MPa}$ and $E^{\infty}_{45/55} = 1.20\,\mathrm{MPa}$), the aluminum grips ($\mathrm{E} \approx 7\,\mathrm{x}\,10^4\,\mathrm{MPa}$) bonded to its surface can be considered rigid. The nature of the highly constrained Solithane sandwiched between the aluminum reinforcements (Figs. 4.1 and 4.2) is such that deformations within these regions can be, to first order, neglected. Thus the physical test specimen, subjected to applied displacements U as indicated in Fig. 5.1a, can be modelled by the simpler bimaterial system shown in Fig. 5.1b, in which the displacements are applied uniformly along the lengthwise boundaries of the specimen. Furthermore, by virtue of the thinness of the specimen, a state of plane stress can be assumed to dominate. For reasons of economy in the analytical counterpart to this experimental work, this latter assumption is critical.[1]

---

[1] Although it is recognized that pure plane stress conditions cannot prevail throughout the entire specimen, it is customary in "thin sheet" problem formulations to make this assumption. The truly three-dimensional stress field at the crack tip is thus simplified. (An interesting consequence of adopting a plane stress assumption in bimaterial problems is the omission of the out-of-plane stresses that arise wholly from the elastic modulus mismatch across the interface. However, the prevailing philosophy maintains that these stresses play a secondary role in determining crack growth behavior for problems of this class, in which the in-plane stresses dominate. Inasmuch as this research constitutes an initial study of interfacial crack growth behavior, it seems reasonable to follow, at least preliminarily, this line of reasoning. Thus, the influence of these out-of-plane stresses shall not be considered here.)

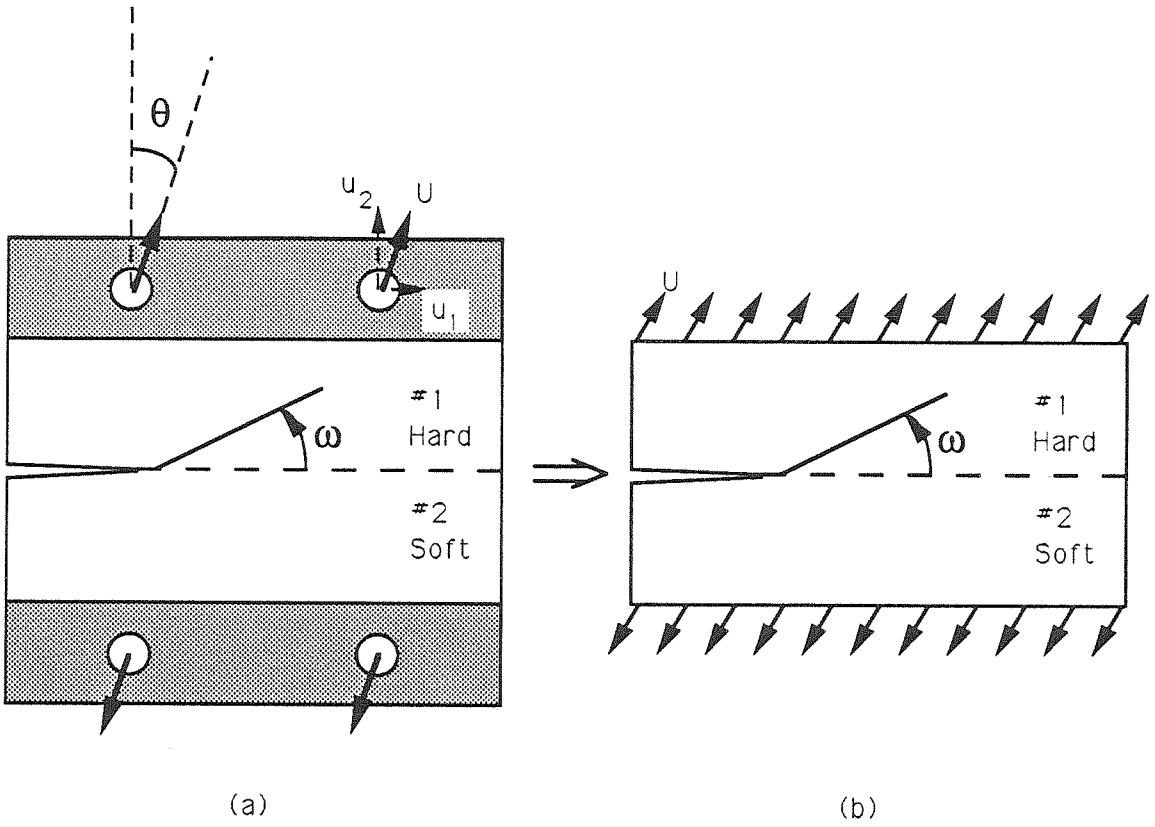

FIG. 5.1 Modelling of specimen subjected to constant applied displacements.

The particular boundary conditions considered here are constant uniform edge displacements, applied suddenly at time zero and held constant thereafter. In order to simplify the analysis, the transients associated with the applied loading are not considered. It is important to note that following the application of the boundary conditions, the edges upon which the displacements are prescribed remain parallel; rotation of these boundaries is not considered.

The applied displacements U may be resolved into components u_1 and u_2, representing displacements parallel and perpendicular to the (undeformed) plane of the interface. These displacements, given by

$$u_1 = U \sin\theta \qquad (5.1.1a)$$

and

$$u_2 = U \cos\theta, \tag{5.1.1b}$$

are prescribed along the entire length of the constrained specimen edges. Hence, an arbitrary combination of far-field tension and shear loadings can be prescribed by suitable adjustment of the loading angle θ.

The near-tip stress fields are dictated by the imposed boundary conditions. The "Finite Element Method" is utilized to compute these near-tip fields, according to the assumptions of linear elasticity and a plane stress problem formulation.[2] In this analysis, the semi-energetic numerical scheme proposed by Matos *et al.* (1989) is utilized. This technique combines information from the nodal crack opening displacements with the values of the J-integral (obtained by the domain integration technique) to extract the two stress intensity factors. It is emphasized that the reference length l used throughout this thesis to "define" K_1 and K_2 (and therefore γ) is $l = 1\,\text{cm}$, *i.e.*, the unit of measure most suitable to the specimen geometry.

In order to perform a comprehensive investigation of the influence of the local fields on crack propagation behavior, a load frame capable of accommodating a large range of the applied loading angle θ is essential. The versatile load frame designed and utilized for this purpose is described in the following section.

---

[2] The workhorse for the numerical computations reported here was the finite element code "FEAP." The mesh employed consists of approximately 2000 four-node bilinear elements concentrically focused at the tip of the crack. The number of elements (and their distribution) was slightly varied depending on the initial length of the crack.

5.2 The Load Frame Assembly

The load frame assembly is presented in Fig. 5.2. The cylindrical adaptors permit the load frame to be rigidly fastened to an MTS testing machine.[3] Owing to the compliance of the fracture specimens, the entire structural assembly, which is composed of aluminum and steel, can be considered rigid. Thus, any vertical displacement imposed on the adaptors by the MTS crosshead is transmitted to the channel grips, to which the specimen is ultimately mounted. As indicated in Fig. 5.2, the crack tip loading is varied by changing the orientation of the specimen relative to the tension axis provided by the test machine.

The load frame and specimen are designed such that the bimaterial interface and the two specimen edges upon which the displacements are prescribed are all parallel to the channel grip reference line that defines the loading angle θ. Thus, a vertical displacement of the channel grips results in boundary displacements both parallel and perpendicular to the (undeformed) interface of the specimen. By varying the inclination of the channel grips, the relative magnitudes of the two displacement components can be adjusted (*cf.* Eq. 5.1.1), thereby altering the near-tip (local) loading conditions.

The orientation of the channel grips, and ultimately of the specimen, is established by adjusting the vertical and horizontal positions of the eyes of the swing bolts. The swing bolts, each with a pitch of 24 threads per inch, permit fine, incremental adjustment of vertical displacement, and hence of angular rotation θ. In order to accommodate small changes in the loading angle, each channel grip is equipped with a pair of adjustable clevises. These clevises allow the grip to be

[3] Axial-torsional load unit model number 358.10; actuator model number 358.xx; transducer model number 11019 with the following load limits: axial : 3300 lb, torsional: 1500 in-lb.

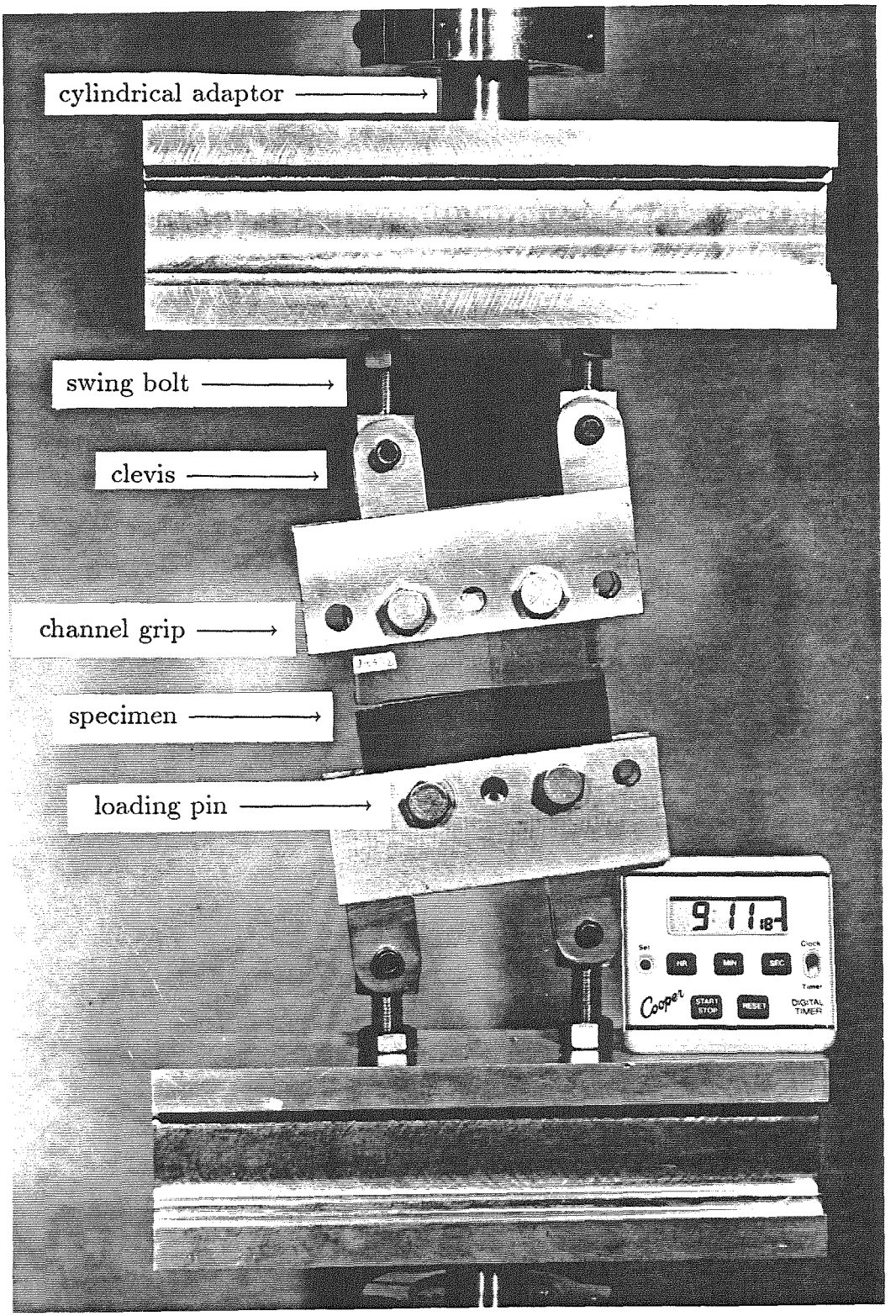

FIG. 5.2 Photograph of the load frame assembly with a mounted specimen.

rigidly fastened to the swing bolts and thus to the frame itself. The movement of each clevis is limited to the plane of the page and is confined to a 2.2 cm slot within the channel grip. This contrivance permits the grip to glide along the ray defined by the angle θ and facilitates mounting the specimen onto the load frame. Once positioned, the location of the grip relative to the clevises is held fixed with set screws.

As the loading angle is increased, rotation of the specimen requires that the swing bolts supporting the grips become progressively more offset with respect to the centerline of the MTS testing machine. For this reason, the frame supports contain several through-thickness, tapped holes along their spans.

The load frame presented in Fig. 5.2 can accommodate loading angles in the range $-71.8° \leq \theta \leq +71.8°$. To achieve angles outside of this range, a pair of simple L-brackets is used in conjunction with classical U-shaped specimen grips (Fig. 5.3). This rudimentary assembly permits loading angles up to nearly $\pm 90°$ to be achieved. However, it should be noted that, with regard to maintaining parallelism of the applied edge displacements, the unsophisticated L-brackets proved to be more cumbersome than the complex load frame illustrated in Fig. 5.2. Thus, pragmatism dictated that the latter load frame become the workhorse for this study, and it was used whenever possible.

5.3 Fracture Testing Procedure

The actual testing procedure used in this experiment is quite straightforward, as described below.

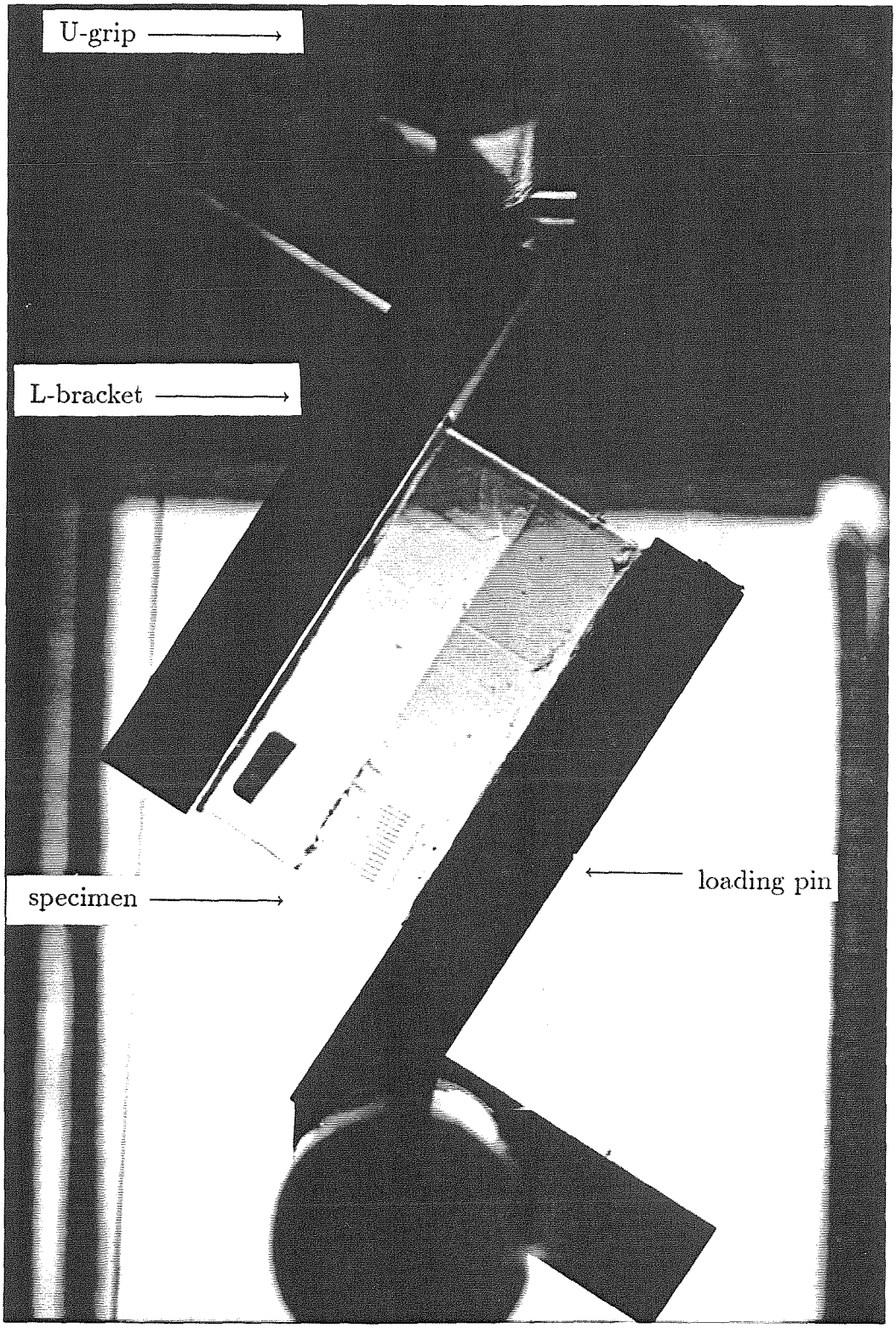

FIG. 5.3 The simple L-bracket load frame assembly (with mounted specimen).

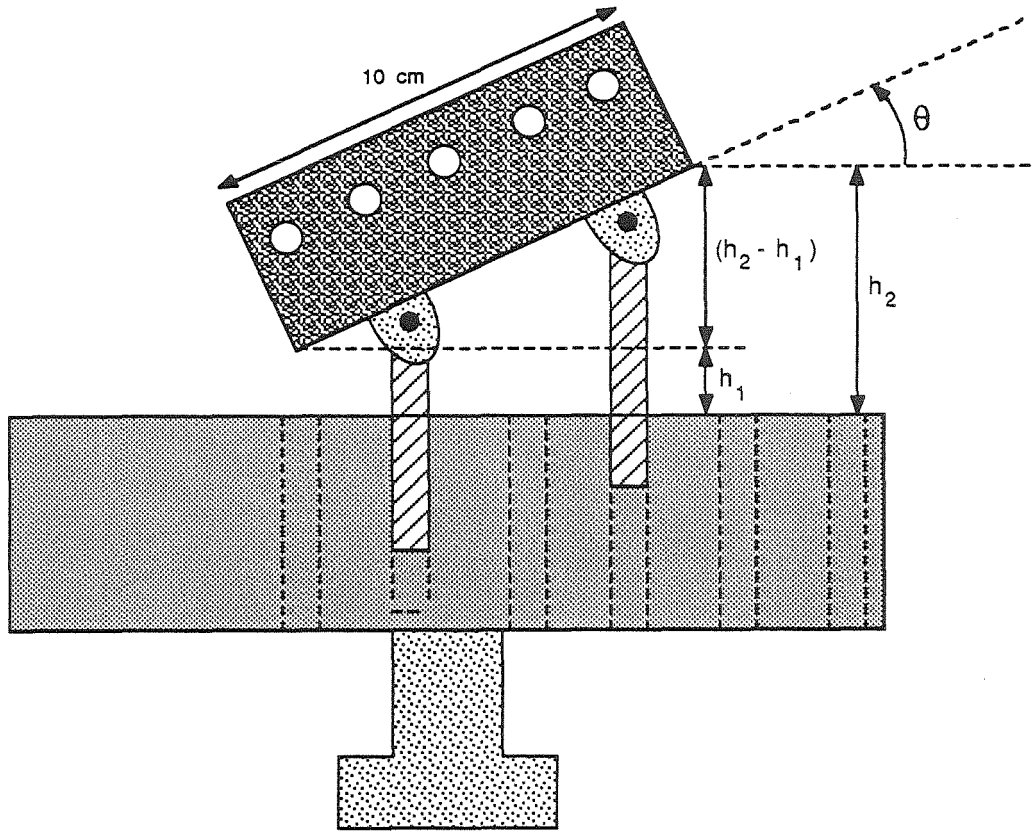

FIG. 5.4 Determination of the loading angle θ.

5.3.1 Mounting the Specimen onto the Load Frame

The first step in mounting the specimen onto the load frame involves fixing the loading angle θ, which is prescribed on the lower half of the load frame by suitable adjustment of the two swing bolts. When the channel grip is rigidly engaged to these bolts via the clevises, the difference in height of the two corners of the lower lengthwise edge of the channel grip satisfies the following condition (Fig. 5.4):

$$\theta = \arcsin\left(\frac{(h_2 - h_1)\ (\text{cm})}{10\ (\text{cm})}\right). \tag{5.3.1}$$

The upper channel grip is similarly adjusted to the appropriate attitude. A suitable fracture specimen is introduced into the load frame by inserting a pair of pins through the appropriate holes in both the lower channel grip and the specimen itself. Since the pins just fit into these holes, there is no "play"; that is, the specimen is held rigidly in place by these pins.

In general, the upper grip will not, *a priori*, be in a position to accommodate the specimen without introducing strain (*i.e.*, the holes in the specimen will not, in general, line up with those in the upper channel grip). Thus, the position of the upper grip must be adjusted such that the holes line up perfectly.

To ensure that no significant prestraining occurs as a result of affixing the specimen to the load frame, and to verify proper specimen alignment, the output of the load cell is monitored as the two pins required to mount the specimen to the upper part of the frame are inserted through the specimen and load frame. Refinements in specimen alignment are performed until neither of the pins results in an applied load in excess of 1 N (typical load levels are ≈ 20 N).[4]

For each fracture test, the trajectory of the advancing crack is documented through periodic photo recording. These photographs can be analyzed to deduce the velocity of the moving crack tip. However, the large field of view employed for these pictures precludes the attainment of resolution sufficient to accurately evaluate the kink angle. Thus, the kink angle is measured in a post-mortem analysis that utilizes an optical comparator. This device permits the origin of the kink to be observed under sufficiently large magnification ($\approx$ 20x). The convention adopted here to define the kink angle ω makes use of the tangent to the crack extension at

[4] For angles in excess of $\pm 71.8°$, the L-brackets (Fig. 5.3) are utilized and the specimen is mounted in a procedure that is entirely analogous to the one described above.

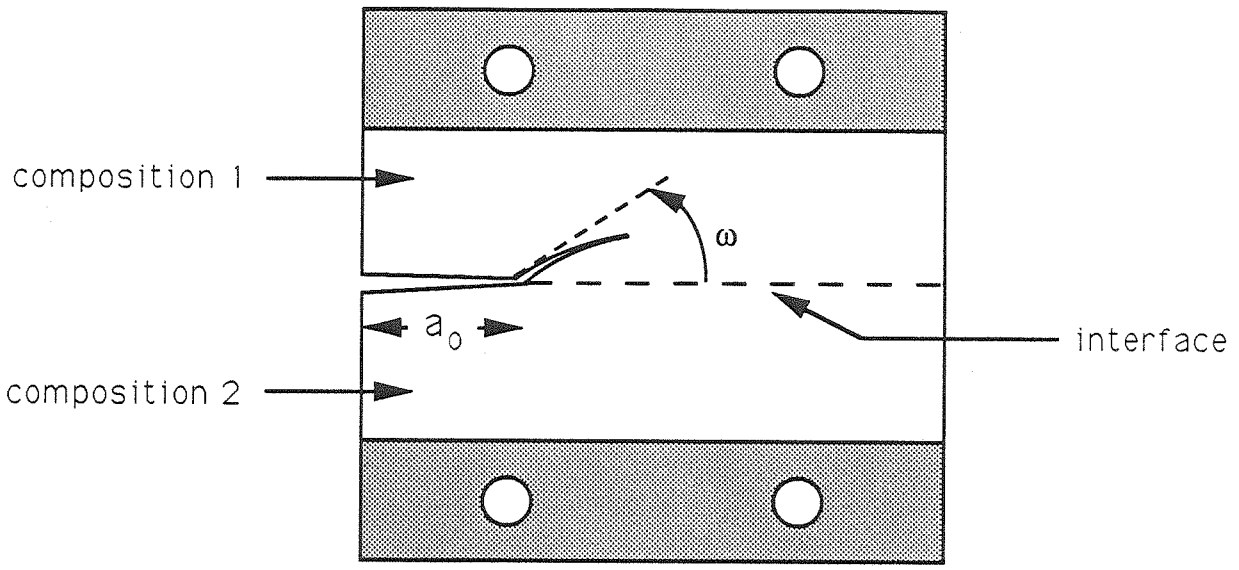

FIG. 5.5 Measurement of experimentally observed kink angle.

the point of deviation from the interface (Fig. 5.5); ω is then the angle between this ray and the plane of the interface, measured positive counterclockwise from the interface, as indicated.

CHAPTER 6

Results

It is convenient to separate the results of this research into two sections. The first, Sec. 6.1, is concerned with the fracture toughness of the bimaterial interface and of the two homogeneous adherends that comprise the bimaterial specimen. In that section, the theoretical developments of Ch. 2 are applied to bimaterial and homogeneous Solithane specimens in order to investigate the influence of the magnitude of the applied loading on the fracture behavior of these specimens. In the second part of this chapter, Sec. 6.2, the kinking behavior of the bimaterial Solithane joint is presented and discussed. In that section, the influence of the shear/tension interaction on the direction of crack propagation relative to the interface is investigated. Thus, in that latter section, attention is focused on the "character" of the loading at the tip of the crack, and not on its magnitude.

6.1 Fracture Toughness

As will be discussed at length in Sec. 6.2, the bimaterial joint was not observed to invariably decohere along the bondline over the complete range of applied loading. Thus, it may be concluded that the strength of the interface is relatively high. In order to quantify this strength and examine its sensitivity to rate effects, an appropriate fracture toughness investigation was developed. For completeness and perspective, this investigation required that the rate dependent fracture toughness of each of the two homogeneous adherends also be characterized.

6.1.1 Characterization of Rate Effects

In order to maintain consistency among the homogeneous and bimaterial specimens with regard to processing variables and crack tip geometry, the "homogeneous" specimens were prepared in a two-step casting procedure that is exactly analogous to the method used to manufacture bimaterial specimens (see Ch. 4). Thus, although the two compositions that form the upper and lower halves of the specimen are now the same material, a possible "interface" between them arises as a consequence of allowing the first material to partially cure before casting the second. In order to clearly delineate this interface, the use of dye in the first-cast composition is continued also in the manufacture of the homogeneous specimens.

For the homogeneous specimens, the loading angle is maintained constant at $\theta = 0°$ in order to allow crack propagation under Mode I conditions along the interface. In contrast, a combination of far-field tension and shear loadings ($\theta \neq 0°$) is required to enforce crack propagation along the interface in the bimaterial specimens. Geubelle and Knauss (1991) have shown (see also Fig. 3.8) that crack propagation along the interface of bimaterial joints may be achieved for a (small) range of loading angles; by trial and error it was determined that $\theta = -15.1°$ and $\theta = -19.8°$ fell within this range (at 25 C) for the bimaterial specimens analyzed here.

Fracture tests were conducted primarily at room temperature (25 C). The applied boundary conditions consisted of constant uniform edge displacements, applied suddenly and held stable thereafter. The magnitude of the applied displacements is varied from test to test, and the resulting stress intensity factor is determined by a finite element code, as discussed in Sec. 5.1. For each specimen, the advancing crack is documented through periodic photo recording. The photographs are analyzed to

deduce the velocity of the moving crack tip; in particular, the slope of the best-fit line through a plot of crack length *vs.* time is used to determine the crack speed.

In order to identify the long-term (slow crack tip velocity) limit, additional tests were performed at 60 C. For the homogeneous specimens, this data was combined with the 25 C data by suitably shifting the observed elevated temperature crack velocities by an appropriate shift factor, in accordance with the WLF equation associated with the theory of viscoelastic material response.[1] The corresponding tests at elevated temperatures for bimaterial interface data did not generate fractures that always followed the interface. It did not appear proper, therefore, to include that data here. Also, additional specimens from another batch were judged to have sufficiently different interface strength to make a comparison questionable.

The resulting data are summarized in Fig. 6.1 in the form of crack tip velocity as a function of the stress intensity factor. Note that the rate-dependent fracture toughness curves for the two homogeneous materials are similar and essentially "parallel," with a shift along the ordinate.

Before proceeding, it is convenient to define as the parameter K_0 the asymptotic value of the stress intensity factor below which crack propagation does not occur. From Fig. 6.1, it is observed that the asymptotic stress intensity factor for the 55/45 composition is $(K_0)_{55/45} = 17 \times 10^{-3}\,\mathrm{MPa}\sqrt{\mathrm{m}}$; for the 45/55 composition, $(K_0)_{45/55} = 5.8 \times 10^{-3}\,\mathrm{MPa}\sqrt{\mathrm{m}}$.

To construct the time-dependent Ψ functions for the two homogeneous materials, one must assemble curves of $\left[\frac{K^2/E^\infty}{\Gamma}\right] = \left[\frac{K^2/E^\infty}{K_0^2/E^\infty}\right] = \left[\frac{K}{K_0}\right]^2$ versus crack

[1] Because a complete characterization of the material behavior of the compositions used here has not been performed, the shift factor was approximated from data for the 50/50 composition investigated by Knauss and Mueller (1967). In this way, the crack speeds observed at 60 C were shifted to lower values by an amount equal to 3.5 decades on a logarithmic scale.

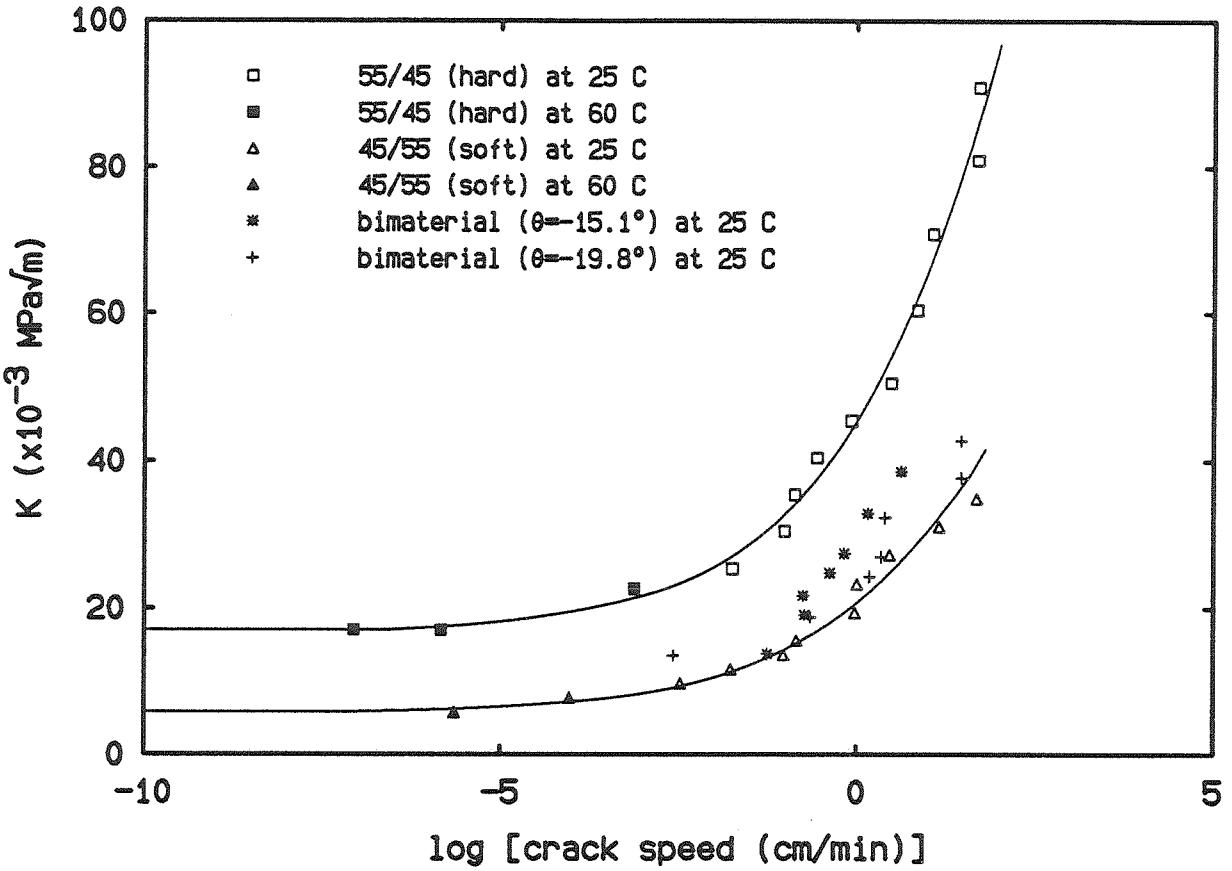

FIG. 6.1 Crack propagation speed as a function of the (absolute) magnitude of the stress intensity factor in the two adherend materials and along the bimaterial interface.

velocity (*cf.* Eq. 2.2.8). For the two homogeneous materials, the functions Ψ_1 and Ψ_2 are shown in Fig. 6.2. In Fig. 6.3, these functions have been combined according to Eq. 2.3.3 to construct Ψ_i, the suggested bimaterial function for the interface. Here the interface data for $\theta = -15.1°$ and $\theta = -19.8°$ have been combined into a single set[2] that is seen to be best fit by Ψ_i when K_0 for the interface assumes the value $(K_0)_{int} = 8 \times 10^{-3}\,\mathrm{MPa}\sqrt{\mathrm{m}}$. The resulting velocity dependent fracture toughness curve for the interface is then shown in Fig. 6.4. According to this latter plot the intrinsic interface strength is intermediate to those of the two homogeneous

[2] The data does not seem to warrant more differentiation.

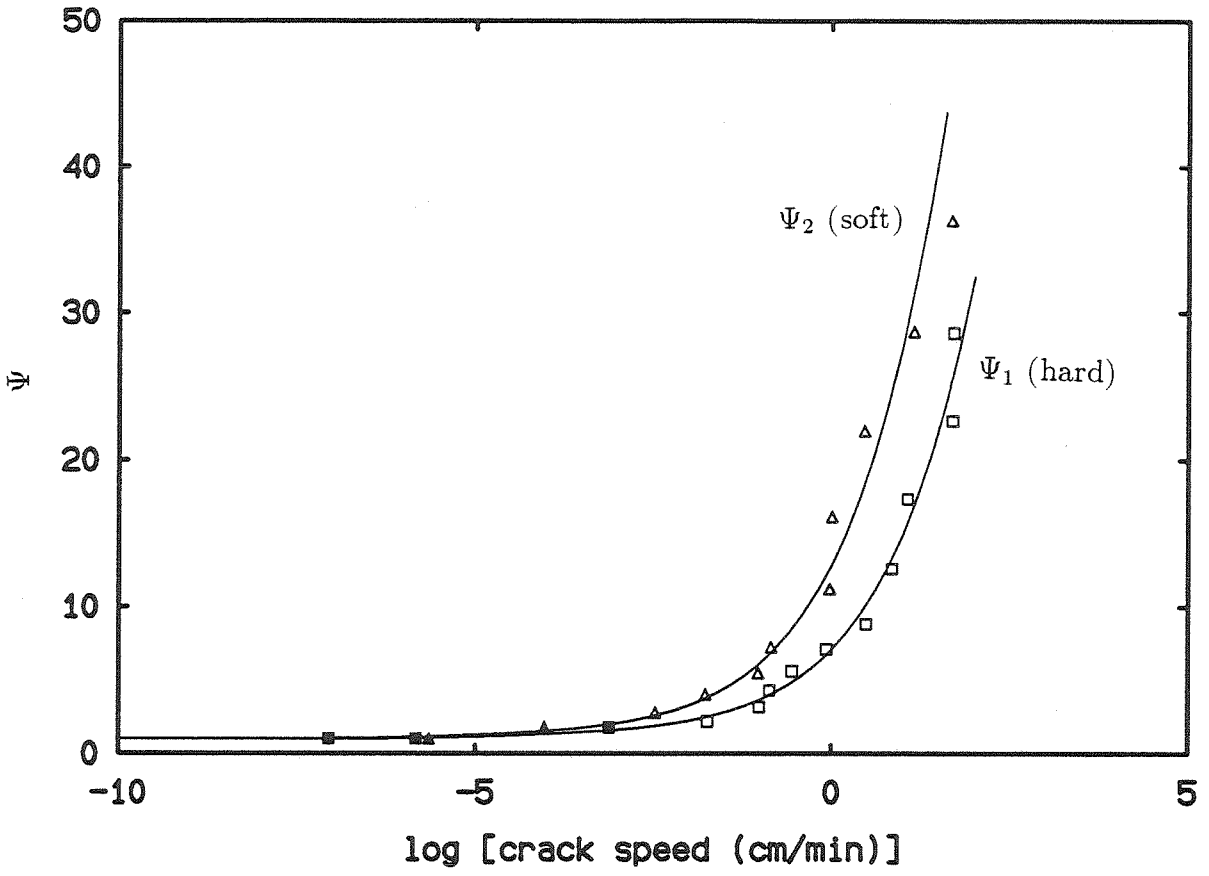

FIG. 6.2 The material Ψ functions for the two solids (*cf.* Eq. 2.2.8).

solids.

6.1.2 Interface Strength

The results presented here support the notion that the "interface strength" has two components: One derives from the viscoelastic contribution embodied in the function Ψ_i and the other from the intrinsic fracture energy Γ_i. Lowering the fracture energy Γ_i will shift the whole curve connecting K or $\left[\frac{K^2}{E^\infty}\right]$ for the interface to lower values. As a consequence, small changes in the intrinsic fracture energy may well induce rates of decohesion that differ by orders of magnitude.

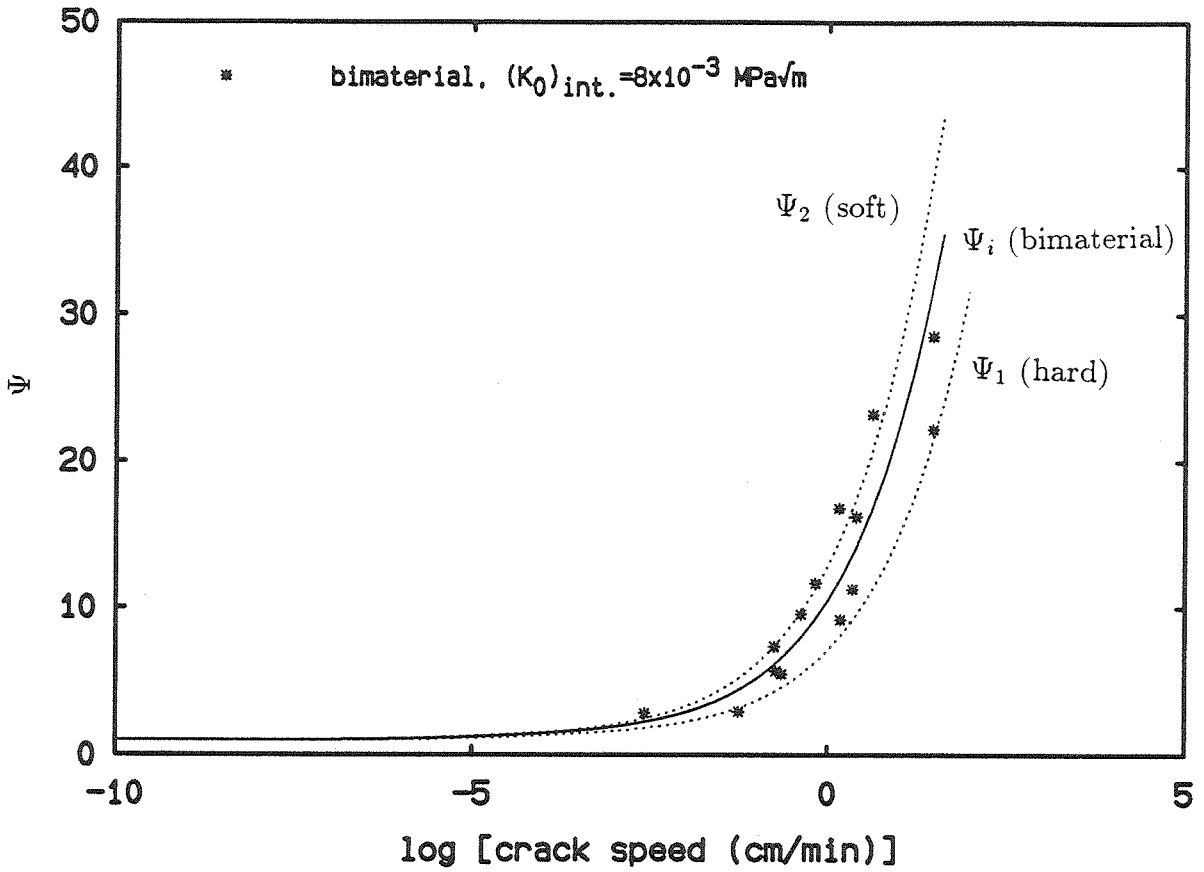

FIG. 6.3 The Ψ function for bimaterial interface fracture. (Experimental points correspond to far-field load angle θ of $-15.1°$ and $-19.8°$.)

As an example, consider the situation for which the "intrinsic interfacial fracture strength" has a value of only one half of that commensurate with the interface data given in Fig. 6.4. For comparison, the velocity dependent fracture energy curves for both the experimentally observed interface and the (hypothetical) reduced strength interface are presented in Fig. 6.5. To see the strong effect that the intrinsic fracture energy has on the speed of decohesion, examine the following two situations. Consider first a stress intensity imposed as indicated by the dotted line denoted by "1". The curve for the interface data indicates that the crack would propagate with a speed of $c_l = 0.17 \, x \, 10^{-3}$ cm/min while the hypothetical (dashed) curve for reduced strength would allow a thousand times higher crack growth rate of

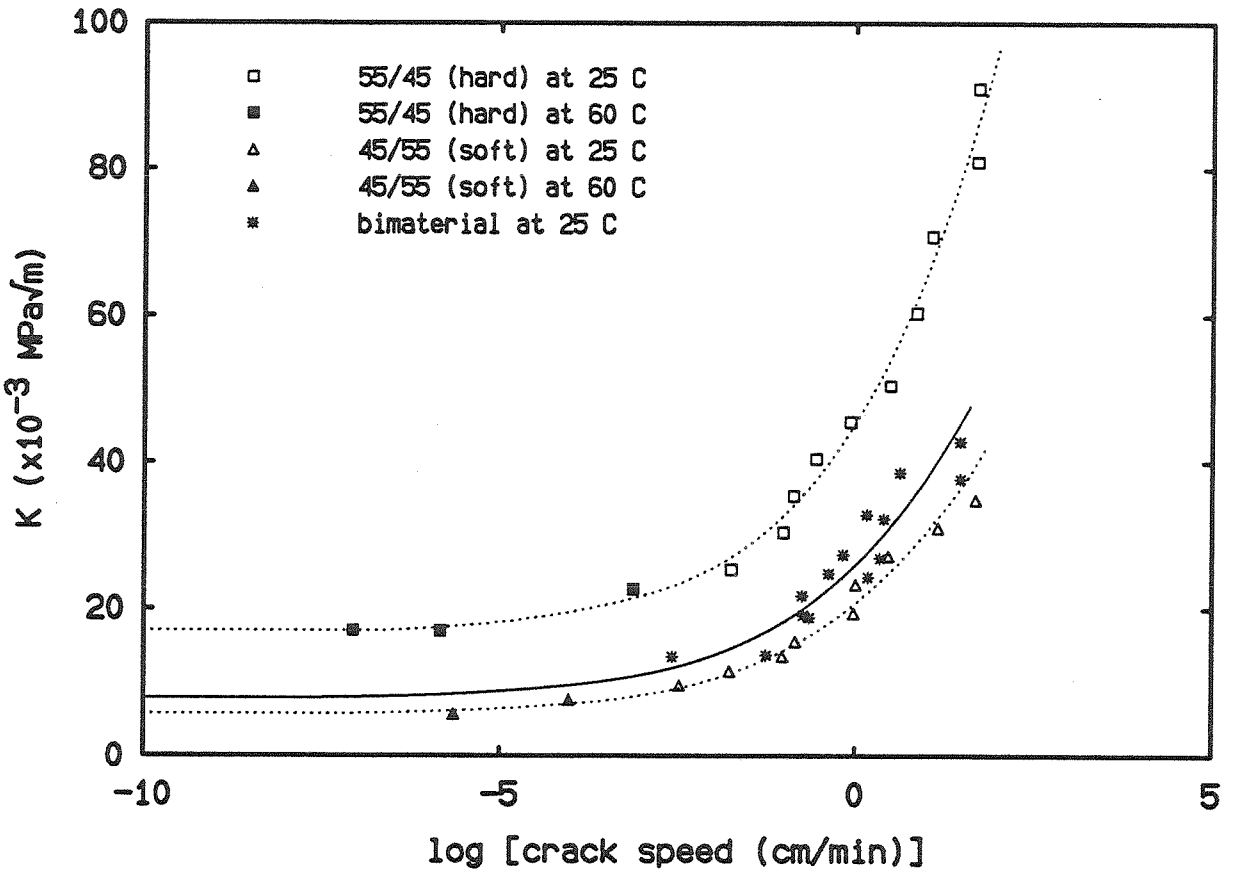

FIG. 6.4 Crack propagation speed as a function of the (absolute) magnitude of the stress intensity factor. (Here the data of Fig. 6.1 are presented along with the computed curve for interfacial fracture.)

$c_h = 0.17$ cm/min. It is clear that a relatively small change in the intrinsic fracture energy (a factor of 1/2) produces a very large change in the speed of crack advance.

To make the point even more explicit, consider as a second example the situation for which the stress intensity factor is represented by the line denoted by "2." Since this value falls below the lowest limit of crack propagation for the experimentally determined interface curve, no fracture would be anticipated at all in this case; on the other hand, for the case of reduced interfacial strength, the crack would indeed advance (and ultimately separate the two materials) at a rate of 0.30×10^{-2} cm/min.

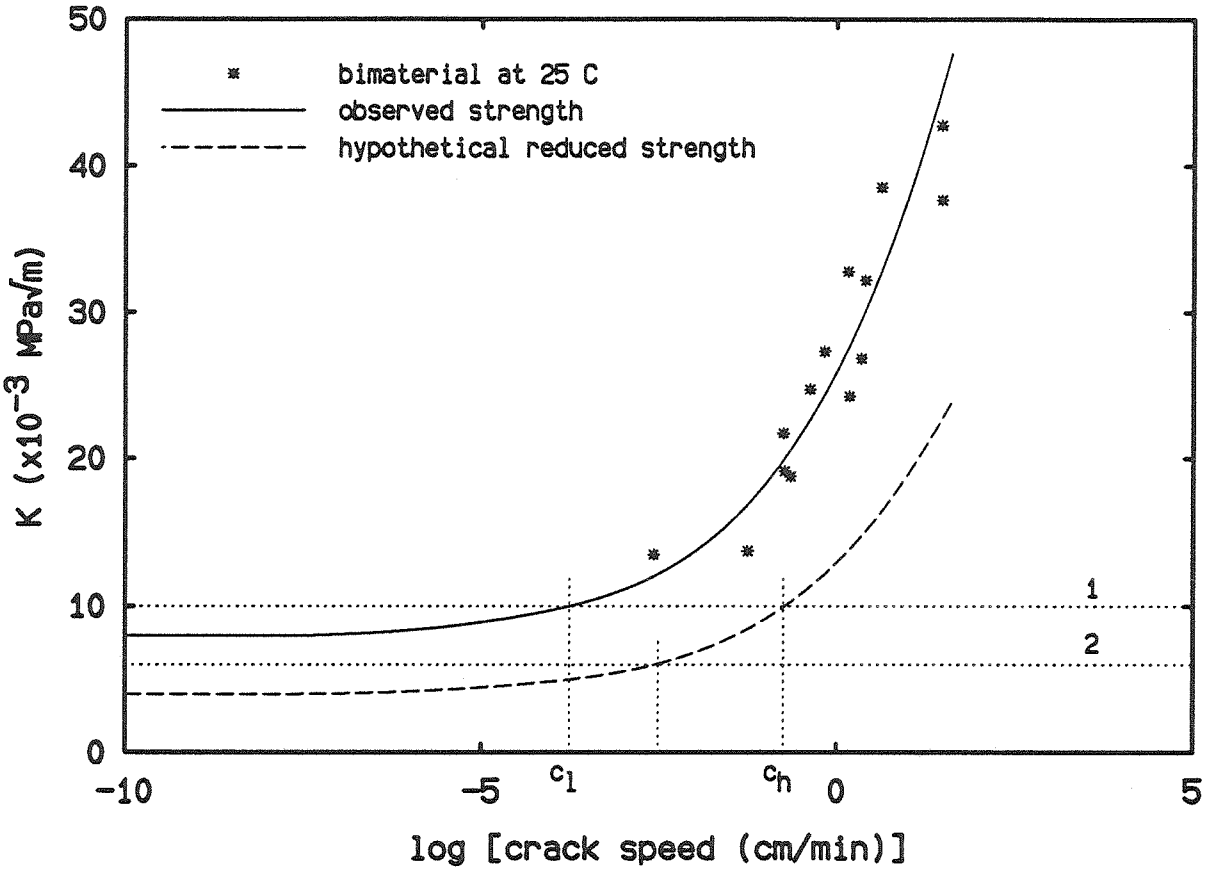

FIG. 6.5 Illustration of the sensitivity of crack speed along an interface to variations in the magnitude of the intrinsic interfacial fracture energy Γ_i.

6.1.2.1 A Relative Measure of Interface Strength

The above scheme of characterizing fracture strength in terms of the stress intensity or energy release rate associated with a velocity dependent function allows a quantitative characterization of a bond strength for viscoelastic materials. It is often also important to establish a measure of bond strength relative to the strength of the adherends, such as when one is interested in optimizing the former. The question arises then as to when the maximum bond strength has been achieved. Figure 6.4 allows a straightforward characterization of this type: It is noted that the intrinsic fracture energy for the interface is higher than that for the softer of

the two materials. It would seem unnecessary in many situations to produce a bond strength that is higher than those of both the materials forming the joint. In this sense then, the bond achieved in the bimaterial specimens would seem to be optimal. Alternately, if the observed bond strength had corresponded to the (hypothetical) curve shown dashed in Fig. 6.5, one would conclude that less than optimal bond strength had been achieved.

This understanding is only clouded by the observation that at the elevated temperature (60 C), the fractures in the bimaterial specimens did not prefer to pass strictly along the interface, but tended instead to follow into the harder of the two materials with a very small angle relative to the interface. The reason for this behavior is not necessarily a failure of the current propositions, but likely a consequence of the process in which the fracture behavior was studied. The loading conditions (global loading angle) that produce crack propagation along the interface were determined by trial and error; it is visible from Fig. 6.1 that a range of several degrees in loading angle produces some, perhaps statistically noticeable, differences at 25 C. It is well possible that the loading condition determined empirically at room temperature was less than totally satisfactory at elevated temperature when the materials respond more rapidly in fracture; in retrospect it would have been advantageous to start with the high temperature tests to determine the loading conditions more distinctly and then proceed to the colder temperatures. As it worked out, there were not enough material specimens left over to re-examine the whole test sequence, except to start with a completely new set of material castings; this is not a trivial task.

It is now of interest to return to the question regarding the magnitude of the size parameter α of the crack tip zone discussed in connection with Eqs. 2.2.1 and

2.3.1. Recall that because of the analytical difficulties with the stress field derived from the linearized theory of (visco)elasticity, there is little hope of defining the parameter appropriate to the bimaterial separation problem analytically. As stated earlier, it has been assumed here that this size parameter is not very different from those for the two adherends, and that curves representing the relation between the available energy and the crack speed are similar and essentially parallel, with a shift along the ordinate in Fig. 6.1. A sizeable difference in the α-parameter would have shown also a strong shift along the *log* $\dot{a}$-axis, with a weaker interface having the effect of shifting the data points to faster crack speeds. This reasoning follows from Eq. 2.2.2, which indicates that a lowering of the cohesive stress σ_0 increases the length α; in order to render the same stress intensity, this increase in α requires that the velocity $\dot{a}$ increase in a similar manner to keep $\left(\frac{\alpha}{\dot{a}}\right)$ constant. Although there is room in the data interpretation to allow for some shifting along the ordinate or the abscissa, there is no strong indication that a pronounced shift along the abscissa has occurred or needs to be considered in the present context.

6.2 Kinking Behavior of the Bimaterial Joint

Under suitable loading conditions, an interface crack may be forced to advance by propagating into one or the other of the adherends rather than along the bondline. This facet of bimaterial interface fracture, known as "crack kinking," is explored in this section. In particular, the influence of the local crack tip loading conditions on the observed kinking behavior is examined.

The kinking behavior of the bimaterial joint was investigated at 25 C and, to a limited extent, at 60 C. Since an elevated temperature provides material rate effects that are higher than those at room temperature, it is expected that a comparison

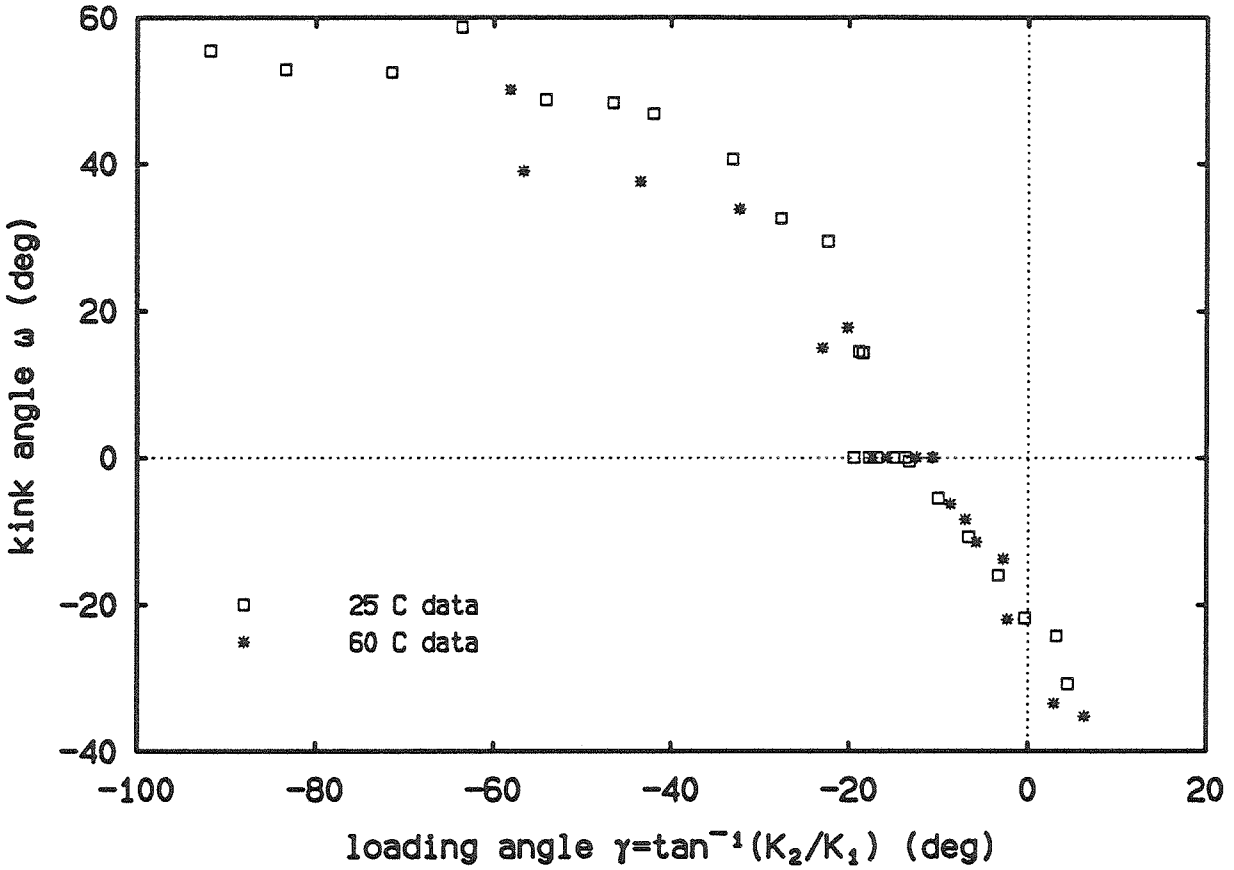

FIG. 6.6 Observed kinking behavior of the bimaterial interface crack.

of the fracture behavior observed at these two distinct temperatures will provide insight into the potential influence of rate effects on the kinking behavior of interface cracks.

For this segment of the investigation, the magnitude of the applied vertical displacement U is maintained constant and only the loading angle θ is permitted to vary from test to test (see Fig. 5.1). For each fracture test, the local loading conditions are characterized by $\gamma = \tan^{-1}(K_2/K_1)$. As discussed in Sec. 5.1, this parameter is computed with a finite element code according to the assumptions of linear elasticity. The reader is reminded that a characteristic length $l = 1\,\text{cm}$ has been chosen in order to numerically "fix" the values of the stress intensity factors.

specimen	a_0 (cm)	θ (deg)	K_1(x10^{-3} MPa$\sqrt{\text{m}}$)	K_2(x10^{-3} MPa$\sqrt{\text{m}}$)	γ (deg)	ω (deg)
W11/2	2.4	0.0	19.73	-2.30	-6.65	-10.8
W11/3	2.3	-8.1	19.42	-3.45	-10.07	-5.5
W11/4	2.4	-15.7	18.81	-4.46	-13.34	0
W11/5	2.2	-24.1	17.72	-5.40	-16.96	0
W11/6	2.3	-28.0	17.09	-5.86	-18.93	14.5
W11/7	2.4	-60.0	9.30	-8.39	-42.04	46.8
W11/8	4.3	-39.0	14.63	-7.66	-27.64	32.7
W11/9	2.5	-50.0	12.17	-7.93	-33.07	40.6
W11/10	2.6	-69.0	6.42	-8.89	-54.14	48.8
W11/11	2.7	-79.0	3.05	-9.10	-71.49	52.5
W11/12	2.3	-89.0	-0.26	-8.17	-91.80	55.5
W12/1a	2.0	-17.0	18.58	-4.52	-13.67	0
W12/1b	2.5	-17.0	18.68	-4.66	-14.02	0
W12/1c	3.1	-16.3	18.74	-4.62	-13.86	0
W12/2	2.1	16.3	19.01	-0.11	-0.35	-21.8
W12/3	2.1	-19.9	18.28	-4.89	-14.97	0
W12/3b	2.9	19.9	18.88	1.04	3.16	-24.2
W12/4	2.2	8.6	19.54	-1.13	-3.32	-16.0
W12/5	2.2	-25.8	17.46	-5.59	-17.77	0
W12/5b	3.5	-26.7	17.23	-6.10	-19.49	0
W12/6	2.1	26.7	17.79	1.37	4.41	-30.7
W12/7	2.1	-27.7	17.13	-5.72	-18.48	14.3
W12/8	2.3	-34.5	15.88	-6.54	-22.39	29.5
W12/9	2.1	34.5	16.50	2.45	8.44	-48.0
W12/10	2.0	-86.0	0.90	-7.72	-83.38	52.9
W13/2	2.3	-76.0	4.19	-8.43	-63.59	58.7
W13/3	2.2	-65.0	7.80	-8.24	-46.57	48.3

TABLE 6.1 Summary of the imposed loading conditions at 25 C.

The fracture behavior of the bimaterial joint at 25 C is presented in Fig. 6.6. For convenience and later reference, the imposed loading conditions for the room temperature data plotted in Fig. 6.6 are reported in Table 6.1. For this series of experiments, the magnitude of the applied (crosshead) displacement U was maintained constant at U = 0.28 cm. For perspective, this displacement represents a gross maximum principal strain between 3.5% and 7%, depending on the magnitude of the far-field loading angle θ, on an uncracked body of the same geometry.

As previously mentioned, the principle of time-temperature trade-off was exploited to examine the influence of rate effects on the observed kinking behavior of

specimen	a_0 (cm)	θ (deg)	K_1(x10^{-3} MPa$\sqrt{\text{m}}$)	K_2(x10^{-3} MPa$\sqrt{\text{m}}$)	γ (deg)	ω (deg)
W21/3	2.6	0.0	18.11	-2.24	-7.06	-8.4
W21/4	3.4	-8.6	17.76	-3.33	-10.63	0
W21/5	2.8	-8.6	17.80	-3.40	-10.81	0
W21/6	2.7	-12.4	17.53	-3.90	-12.54	0
W21/7	2.2	12.4	17.74	-0.72	-2.34	-22.0
W21/8	2.5	-19.6	16.82	-4.75	-15.78	0
W21/9	3.2	19.6	17.36	0.87	2.87	-33.4
W21/10	2.3	-23.6	16.30	-5.13	-17.47	0
W21/11	4.0	23.6	16.89	1.84	6.23	-35.2
W21/12	3.2	8.05	18.06	-0.88	-2.79	-13.8
W21/13	2.4	3.44	18.08	-1.85	-5.85	-11.5
W21/14	2.4	-3.44	18.00	-2.76	-8.73	-6.3
W21/15	2.6	-28.5	15.57	-5.74	-20.23	17.75
W22/10	2.2	-35.1	14.42	-6.13	-23.04	15.0
W22/11	2.4	-48.6	11.47	-7.26	-32.32	33.9
W22/13	2.5	-60.5	8.33	-7.91	-43.52	37.6
W22/14	3.5	-68.4	5.86	-8.90	-56.65	39.0
W22/15	2.5	-71.8	5.02	-8.08	-58.17	50.1

TABLE 6.2 Summary of the imposed loading conditions at 60 C.

the bimaterial joint, albeit to a limited extent. The tests for this characterization were performed at 60 C under an imposed displacement U = 0.256 cm, which represents a 3.2%-6.4% gross maximum principal strain, depending on θ. The kinking behavior observed for this set of experiments is presented along with that of the 25 C tests in Fig. 6.6; pertinent information regarding the imposed loading conditions for the elevated temperature tests is compiled in Table 6.2.

The nominal applied strains, and thus the near-tip conditions, are very similar for both sets of data presented (*cf.* Tables 6.1 and 6.2). However, because of the disparity in testing temperatures, the material rate conditions are significantly different between the two. Since the two sets of data presented in Fig. 6.6 show essential agreement within experimental accuracy, one concludes that rate effects do not significantly affect the direction of crack propagation, at least for the (small) strain levels studied here.

6.2.1 Comparison with Analytical Results

It is informative to compare the experimentally observed kinking behavior with various numerical predictions. In Fig. 6.7, the experimental data is presented along with analytical (small strain) results determined numerically by Geubelle and Knauss (1991). Although the numerical and experimental data do exhibit the same trend, they do not agree uniformly. In particular it is noted, in contrast to the homogeneous case, that both the experimental and analytical results yield crack propagation along the interface ($\omega = 0$) for a finite range of load mixity γ rather than for only a single value of this parameter.

The analytical plot in Fig. 6.7 is predicated upon the maximum energy release rate criterion that is widely accepted as a basic concept in the fracture analysis of homogeneous bodies. For the case of an interface crack, Geubelle and Knauss (1991) have demonstrated that the energy release rate is non-unique (see also Ch. 3); in contrast to the homogeneous case, this quantity depends in the bimaterial formulation on the magnitude of the (virtual) crack extension Δl that is commissioned for computational purposes. Figure 6.7 presents the so-called "master curve" for crack kinking; it has been calculated for $\left(\frac{\Delta l}{l}\right) = 1$. (Recall that l is the reference length used to "define" the stress intensities; here $l = 1\,\text{cm}$.) It should also be noted that the master curve in Fig. 6.7 is predicated upon the assumption that the fracture toughness of each solid and of the interface itself are equal and independent of load mixity (*i.e.*, independent of γ).

A significant shortcoming of the analytical result is its inability to match the experimental data for that region of applied loading that corresponds to crack advance along the interface ($\omega = 0$). If this region could be predicted for a given material pair, a useful evaluation of potential joint failure could be made: In many

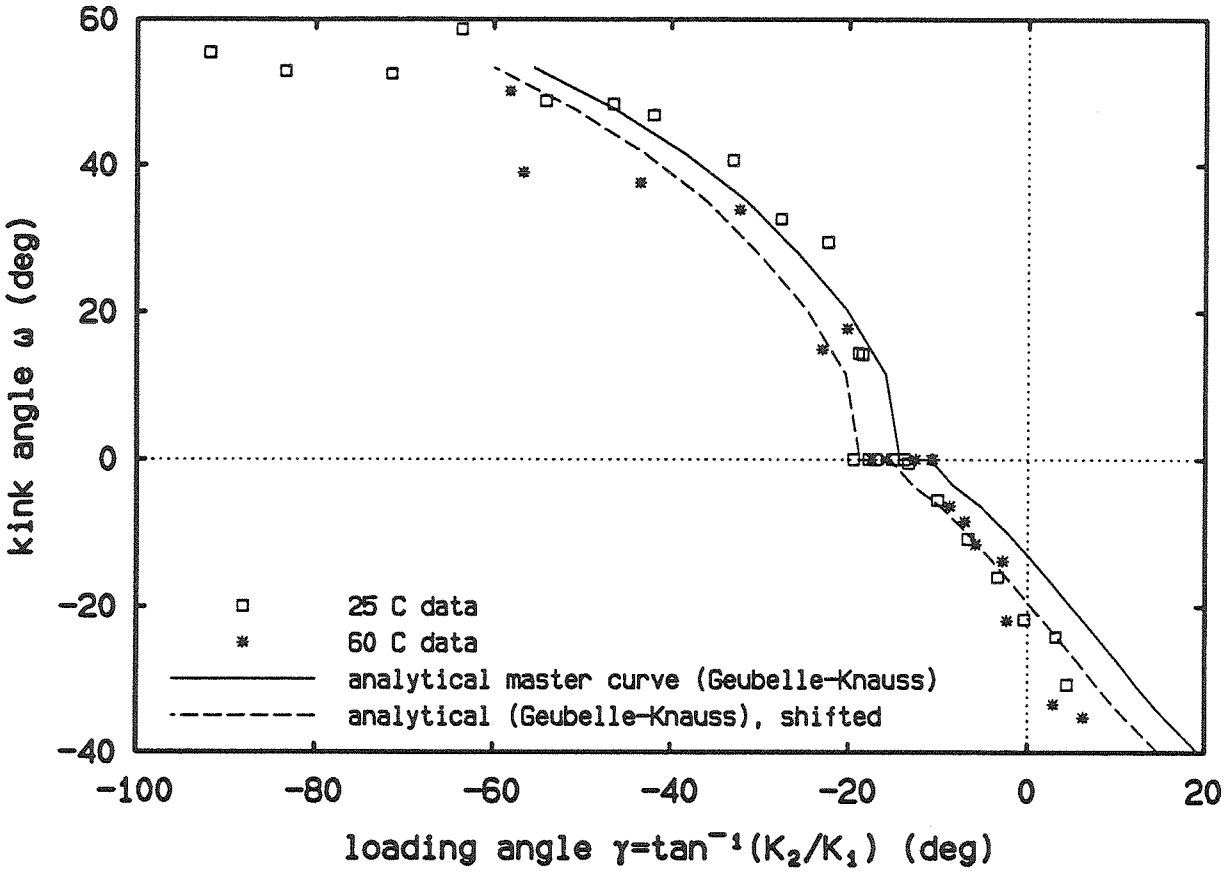

FIG. 6.7 Comparison of experimental and analytical results.

situations, it is necessary only to determine which of the two materials is likely to fail under expected or anticipated loading conditions. A precise prediction of the propagation direction of an interface crack in a structural component might then be unnecessary, especially in light of the assumptions that must typically be made in evaluating the potential loads that may be encountered by a part in service.

As a consequence of the non-uniqueness of the energy release rate, the numerical plot of kink angle ω *vs.* phase angle γ can be shifted along the abscissa simply by choosing an "appropriate" length of the crack extension Δl. Suitable manipulation of this parameter yields the "shifted" plot presented in Fig. 6.7, in which $\Delta l^* = 1.1\,\text{mm}$. In moving experiment and analysis into closer agreement by choosing such

a characteristic length, the argument has been advanced that this length should represent a measure of the material microstructure that dominates the fracture process. It is emphasized, however, that such a length specification is not part of the analytical modelling; such a specification would thus constitute, in some way, a "retrofit" of the analysis. Moreover, it is noted that the microstructure of the materials involved in this study is significantly smaller than the 1.1 mm size scale needed to make analysis and experiment agree. Thus, although in other instances the magnitude of Δl may seem indicative of a damage-related parameter, it appears from this work that a strong physical interpretation of this parameter is not reasonable at this time.

6.2.2 Observations on the Kink Geometry

In those instances when the crack was observed to kink away from the interface and into either of the adjacent materials, a post-mortem analysis of the crack initiation site revealed that the crack tip, with two exceptions discussed below, deviated abruptly away from the interface at the point of initiation. The kinking behavior was thus manifest immediately and did not develop over a finite distance as crack growth proceeded. Furthermore, the initial deviation from the interface represents the largest angle that the direction of the crack tip made with respect to the interface. As the crack tip propagated away from its point of initiation, it was generally observed to curve towards the interface and tended to approach a path perpendicular to the applied displacements (see Fig. 5.5). This behavior is consistent with that observed by Erdogan and Sih (1963) in their study of an angled crack in a homogeneous sheet subjected to applied loads that are not normal to the axis of the crack.

Under one loading condition, however, the kink failed to establish itself immediately. It was observed that for the smallest negative value of the far-field loading angle θ required to initiate crack advance into material 1 (the stiffer of the two materials), corresponding to $\gamma \approx -19°$ at 25 C and $\gamma \approx -20°$ at 60 C, the angle between the direction of the advancing crack tip and the interface approached the "expected" (maximum) value only gradually. (The reported angle represents this maximum value.) In these instances, the kinking behavior required a finite distance ($\approx 3-5$ mm) to develop. Since this behavior was observed for this loading condition at 25 C and at 60 C (2 total data points), it may not be anomalous. Rather, it is believed to be indicative of the finite "thickness" of the physical interfacial region. For analytical purposes, this thickness is assumed to be infinitesimal; in reality, however, some interdiffusion of the two compositions must occur during specimen co-curing. As a consequence of this interdiffusion, a very small but finite transition region develops between the two materials. For the loading conditions mentioned above, the finite extent of the interfacial region appears to temper the favored kink direction, and the kink requires a small extension over which to fully develop. It is noted that subsequent to kinking, the crack paths in these instances were also observed to curve towards the interface and ultimately tended towards the direction normal to the applied displacements.

6.2.3 Observations on Crack Propagation Rates

Although a formal investigation of the rates of crack propagation into the adherends following crack kinking was not undertaken, some observations on this topic are worth reporting. First, rates of crack propagation into material 2 (Solithane 45/55, the softer of the two adherends) and along the interface were comparable

and substantially higher than those observed for crack advance into material 1 (the 55/45 composition). (This behavior is expected on the basis of the viscoelastic characteristics of the two materials.) At room temperature, for example, crack advance into material 2 typically proceeded at a rate of several mm per minute or faster, and the duration of complete fracture tests under such conditions was generally on the order of a few minutes. In contrast, the rate of crack propagation into material 1 at room temperature was on the order of hours per mm of crack advance. Thus, in order to allow for sufficient crack growth into the stiffer (more viscous) material, each of these fracture tests was generally performed over the course of many hours. Although the fractures were observed to proceed more rapidly at 60 C than at room temperature, a discernible difference among crack propagation rates was noticed also with the specimens tested at elevated temperature.

A second important observation is that crack speeds tended to decrease as the Mode II component increased relative to Mode I: As the magnitude of the observed kink angle ω increased, the fracture tests required progressively longer durations to allow for sufficient crack growth to occur. One explanation for this observed response is that the magnitude of the gross "opening mode" stresses is less for large kink angles than for small ones, and the propensity for crack advance is consequently diminished.

CHAPTER 7

Conclusions

The fracture behavior of a bimaterial joint with a crack located along its interface was investigated. Because the strength of the interface exerts a profound influence on the ultimate fracture behavior of the joint, it was essential to first characterize the toughness of this interface. This assessment was made in the context of viscoelasticity. In particular, it has been demonstrated that the time dependent unbonding of two joined viscoelastic solids follows a rate dependent fracture process that can be described to a large extent by the viscoelastic properties of the two adherends; moreover, the strength of the bond can be characterized in terms of an equilibrium fracture energy, the magnitude of which characterizes the bond strength quantitatively. In addition, that interfacial and intrinsic fracture strength provides a measure of the quality of the bond as compared to the strength of either of the two adherends, in particular with respect to the weaker of the two. While the range of viscoelastic properties represented by the materials studied is not very wide, it appears that the model of viscoelastic interface failure proposed by Knauss (1971), derived from essentially elastic fracture mechanics by viscoelastic analogy, has practical merit.

Following the evaluation of specimen interface toughness, attention was focused on characterizing the propensity of an interface crack to kink out of the interface upon loading. It has been demonstrated that the crack could be made to advance

into either of the two adherends or along the interface itself, depending on the character of the applied loading conditions. In particular, crack propagation along the interface was observed to occur for a finite range of load mixity, a phenomenon predicted by linearly elastic analysis of the bimaterial joint but absent from the corresponding homogeneous development. Agreement between numerical analysis and experimental observations can be improved by suitable choice of a length parameter corresponding to the initial (virtual) crack extension. This parameter is not a part of the fracture model *per se*, but rather a retrofit parameter required to bring analysis into closer agreement with the observed kinking behavior. Similarity in the fracture data garnered from tests performed at 25 C and at 60 C indicate that rate effects do not significantly influence the kinking behavior of the joints studied here.

It would be appropriate in a follow-on study of either aspect of interfacial fracture presented here to examine the consequences of employing a more distinctly different set of materials (after one has learned how to control the interface strength of such a material combination). An additional suggestion for future work would be to duplicate the methodology employed in this investigation for a bimaterial system in which only the intrinsic interfacial fracture strength is varied. Such experiments could: (*i*) help validate the general applicability of Knauss' (1971) model for the case of interfacial separation; and (*ii*) provide further insight into the kinking behavior of interface cracks, including the significance of the finite range of load mixity which results in bondline decohesion.

References

Bowen, J. M., 1990, "Preparation of a Bimaterial Fracture Specimen Composed of Solithane 113," GALCIT SM Report 90-25, Graduate Aeronautical Laboratories, California Institute of Technology, Pasadena, California, 91125.

Bowen, J. M., 1991, "Crack Initiation and Propagation at the Interface Between Viscoelastic Solids," GALCIT Ae200 Report (Fall 1990-91), Graduate Aeronautical Laboratories, California Institute of Technology, Pasadena, California, 91125.

Dundurs, J., 1969, "Edge-Bonded Dissimilar Orthogonal Elastic Wedges under Normal and Shear Loading," *ASME Journal of Applied Mechanics*, Vol. 36, pp. 650-652.

Erdogan, F., and Sih, G. C., 1963, "On the Crack Extension in Plates Under Plane Loading and Transverse Shear," *J. Basic Engrg., Trans.*, Vol. 85, pp. 519-527.

Evans, A. G., and Hutchinson, J. W., 1989, "Effects of Non-planarity on the Mixed Mode Fracture Resistance of Bimaterial Interfaces," *Acta metall.*, Vol. 37, No. 3, pp. 909-916.

Geubelle, P. H., and Knauss, W. G., 1991, "Crack Propagation at and near Bimaterial Interfaces: Linear Analysis," GALCIT SM Report 91-17, Graduate Aeronautical Laboratories, California Institute of Technology, Pasadena, California, 91125.

Greensmith, H. W., 1956, "Rupture of Rubber, IV. Tear Properties of Vulcanizates Containing Carbon Black," *Journal of Polymer Science*, Vol. 21, pp. 175-187.

Greensmith, H. W., 1960, "Rupture of Rubber, VIII. Composite of Tear and Tensile Rupture Measurements," *Journal of Applied Polymer Science*, Vol. 3, No. 8, pp. 183-193.

He, M.-Y., and Hutchinson, J. W., 1988, "Crack Deflection at an Interface Between Dissimilar Elastic Materials," Harvard University Report MECH-133.

He, M.-Y., and Hutchinson, J. W., 1989, "Kinking of a Crack Out of an Interface," *ASME Journal of Applied Mechanics*, Vol. 56, pp. 270-278.

Hutchinson, J. W., 1989, "Mixed Mode Fracture Mechanics of Interfaces," Harvard University Report MECH-139.

Hutchinson, J. W., Mear, M. E., and Rice, J. R., 1987, "Crack Paralleling an Interface Between Dissimilar Materials," *ASME Journal of Applied Mechanics*, Vol. 54, pp. 828-832.

Knauss, W. G., 1971, "Fracture Mechanics and the Time Dependent Strength of Adhesive Joints," *J. Composite Materials*, Vol. 5, pp. 176-192.

Knauss, W. G., 1974, "On the Steady Propagation of a Crack in a Viscoelastic Sheet: Experiments and Analysis," in *Deformation and Fracture of High Polymers*, Kausch, Hassell, and Jaffee (Eds.), Plenum Press, pp. 501-541; also available as GALCIT SM Report 73-2, Graduate Aeronautical Laboratories, California Institute of Technology, Pasadena, California, 91125.

Knauss, W. G., 1976, "Fracture of Solids Possessing Deformation Rate Sensitive Material Properties," *The Mechanics of Fracture*, F. Erdogan, ed., ASME, NY, AMD Vol. 19, December 1976.

Knauss, W. G., 1988, "An Investigation of Viscoelastic Fracture Near and At Interfaces," AFAL-TR-88-083.

Knauss, W. G., and Dietmann, H., 1970, "Crack Propagation Under Variable Load Histories in Linearly Viscoelastic Solids," *Int. J. Engrg. Sci.*, Vol. 8, pp. 643-656.

Knauss, W. G., Geubelle, P. H., and Bowen, J. M., 1991, "Fracture At and Near the Interface Between Two Viscoelastic Solids," GALCIT SM Report 91-20, Graduate Aeronautical Laboratories, California Institute of Technology, Pasadena, California, 91125.

Knauss, W. G., and Mueller, H. K., 1971, "Crack Propagation in a Linearly Viscoelastic Strip," *Journal of Applied Mechanics*, Vol. 38, Series E, p. 483.

Knauss, W. G., and Mueller, H. K., 1967, "The Mechanical Characterization of Solithane 113 in the Swollen and Unswollen State," AFRPL-TR-68-125 or GALCIT SM Report 67-8, Graduate Aeronautical Laboratories, California Institute of Technology, Pasadena, California, 91125.

Lake, G. J., and Thomas, A. C., 1967, "The Strength of Highly Elastic Materials," *Proc. Royal Soc. of London*, Vol. 300, August 1967, pp. 108-119.

Matos, P. P. L., McMeeking, R. M., Charalambides, P. G., and Drory, M. D., 1989, "A method for calculating stress intensities in bimaterial fracture," *Int. J. Fract.*, Vol. 40 (1989), pp. 235-254.

Mazor, E., and Bowen, J. M., 1989, "Crack Propagation At and Near Interfaces of Viscoelastic Solids," GALCIT Ae 100 Report, December 1989, Graduate Aeronautical Laboratories, California Institute of Technology, Pasadena, California, 91125.

Mazor, E., and Bowen, J. M., 1990, "Material Selection: An Investigation of the Mechanical Properties and the Aging Behavior of Solithane 113," GALCIT Ae 100 Report, April 1990, Graduate Aeronautical Laboratories, California Institute of Technology, Pasadena, California, 91125.

Mukai, D. J., Ballarini, R., and Miller, G. R., 1990, "Analysis of Branched Interface Cracks," *ASME Journal of Applied Mechanics*, Vol. 57, pp. 887-893.

Rice, J. R., 1988, "Elastic Fracture Mechanics Concepts for Interfacial Cracks," *ASME Journal of Applied Mechanics*, Vol. 55, pp. 98-103.

Rice, J. R., and Sih, G. C., 1965, "Plane Problems of Cracks in Dissimilar Media," *ASME Journal of Applied Mechanics*, June 1965, pp. 418-423.

Schapery, R. A., 1975, "A Theory of Crack Initiation and Growth in Viscoelastic Media: I. Theoretical Development, (p. 141), II. Approximate Methods of Analysis, (p. 369), III. Analysis of Continuous Growth, (p. 549)," *International Journal of Fracture*, Vol. 11, 1975.

Suo, Z., and Hutchinson, J. W., 1988, "Steady-State Cracking in Brittle Substrates Beneath Adherent Films," Harvard University Report, MECH-132.

Suo, Z., and Hutchinson, J. W., 1989, "Sandwich Test Specimens for Measuring Interface Crack Toughness," *Materials Science and Engineering*, Vol. A107, pp. 135-143.

Symington, M. F., 1987, "Eigenvalues for Interface Cracks in Linear Elasticity," *ASME Journal of Applied Mechanics*, Vol. 54, pp. 973-974.

Williams, M. L., 1952, "Stress Singularities Resulting From Various Boundary Conditions in Angular Corners of Plates in Extension," *ASME Journal of Applied Mechanics*, Dec. 1952, pp. 526-528.

Williams, M. L., 1956a, "On the Stress Distribution at the Base of a Stationary Crack," *ASME Journal of Applied Mechanics*, March 1956.

Williams, M. L., 1956b, "The Complex-Variable Approach to Stress Singularities - II," *ASME Journal of Applied Mechanics*, Sept. 1956, pp. 477-478.

Williams, M. L., 1959, "The Stresses Around a Fault or Crack in Dissimilar Media," *Bulletin of the Seismological Society of America*, Vol. 49, No. 2, pp. 199-204.